

Performance of the CMS drift tube chambers with cosmic rays

To cite this article: CMS Collaboration 2010 *JINST* **5** T03015

View the [article online](#) for updates and enhancements.

Related content

- [Calibration of the CMS drift tube chambers and measurement of the drift velocity with cosmic rays](#)
CMS Collaboration
- [Performance of the CMS drift-tube chamber local trigger with cosmic rays](#)
CMS Collaboration
- [Fine synchronization of the CMS muon drift-tube local trigger using cosmic rays](#)
CMS Collaboration

Recent citations

- [Design and Description of the CMS Magnetic System Model](#)
Vyacheslav Klyukhin
- [Stopping quirks at the LHC](#)
Jared A. Evans and Markus A. Luty
- [FPGA-based algorithms for the new trigger system for the phase 2 upgrade of the CMS drift tubes detector](#)
J.-M. Cela-Ruiz



The Electrochemical Society
Advancing solid state & electrochemical science & technology
2021 Virtual Education

Intensive Short Courses

Sunday, October 10 & Monday, October 11

Providing students and professionals with in-depth education on a wide range of topics

[CLICK HERE TO REGISTER](#)



RECEIVED: November 26, 2009

REVISED: January 26, 2010

ACCEPTED: January 29, 2010

PUBLISHED: March 19, 2010

COMMISSIONING OF THE CMS EXPERIMENT WITH COSMIC RAYS

Performance of the CMS drift tube chambers with cosmic rays

CMS Collaboration

ABSTRACT: Studies of the performance of the CMS drift tube barrel muon system are described, with results based on data collected during the CMS Cosmic Run at Four Tesla. For most of these data, the solenoidal magnet was operated with a central field of 3.8 T. The analysis of data from 246 out of a total of 250 chambers indicates a very good muon reconstruction capability, with a coordinate resolution for a single hit of about $260\ \mu\text{m}$, and a nearly 100% efficiency for the drift tube cells. The resolution of the track direction measured in the bending plane is about 1.8 mrad, and the efficiency to reconstruct a segment in a single chamber is higher than 99%. The CMS simulation of cosmic rays reproduces well the performance of the barrel muon detector.

KEYWORDS: Large detector systems for particle and astroparticle physics; Particle tracking detectors (Gaseous detectors)

ARXIV EPRINT: [0911.4855](https://arxiv.org/abs/0911.4855)

Contents

1	Introduction	1
2	DT chamber setup and trigger conditions	2
3	Monte Carlo simulation of cosmic ray data	4
4	Local reconstruction of muon tracks	6
5	Reconstructed hits in DT chambers	7
5.1	Spatial resolution	7
5.2	Hit reconstruction efficiency	12
6	Reconstructed track segments in DT chambers	12
6.1	Multiplicity of associated hits and track segment efficiency	12
6.2	Track segment position and direction measurements	24
6.3	Bending power measurements	25
7	Conclusions	27
	The CMS collaboration	31

1 Introduction

The primary goal of the Compact Muon Solenoid (CMS) experiment [1] is to explore particle physics at the TeV energy scale, exploiting the proton-proton collisions delivered by the Large Hadron Collider (LHC) at CERN. The central feature of the Compact Muon Solenoid apparatus is a superconducting solenoid, of 6 m internal diameter, providing a field of 3.8 T. Within the field volume are the silicon pixel and strip tracking detectors, the crystal electromagnetic calorimeter and the brass/scintillator hadron calorimeter. Muons are measured in gas-ionization detectors embedded in the steel return yoke. In addition to the barrel and endcap detectors, CMS has extensive forward calorimetry.

In autumn of 2008, after closing the CMS detector in preparation for the LHC start-up and the first underground test of the magnet, CMS undertook a long period (about 1 month) of data taking, collecting about 270 million cosmic ray events with varying detector and trigger conditions. Data were collected both without and with magnetic field (at various values of the current in the coil of the solenoid). In this “Cosmic Run At Four Tesla” (CRAFT), the large majority of the data were collected with a magnetic field of $B = 3.8$ T in the volume of the solenoid. Almost all CMS sub-detectors were active and included in the data acquisition [2].

In summer 2006, cosmic ray data were taken on the surface with the detector closed, the “Magnet Test and Cosmic Challenge” (MTCC) [3]. In that period only a small part (about 5%) of the muon detector was equipped for readout, and the tracking detectors were not installed inside the coil. Many results on the muon detector performance [4] and measurements of physical quantities related to the cosmic ray properties [5] were obtained. The CRAFT exercise allowed the extension of those studies of muon reconstruction and identification to the entire system, and in much greater detail.

This paper addresses muon reconstruction in the drift tube chambers of the barrel muon system, hereafter referred to as “DT chambers”, focusing on the reconstruction of local hits and track segments in the chambers. Information from this reconstruction, together with the output of the local reconstruction of other CMS subsystems, is used as input to the following stage of the global muon reconstruction [6]. Detailed comparisons of different track segments belonging to the same track, but measured in different stations, were performed, using in addition information from the internal tracking devices. The non-bunched structure of the cosmic rays affects the time measurements in the DT cells and hence the position resolution obtained in the initial stage of the reconstruction process. Despite this, and the fact that cosmic rays illuminate a large part of the detector quite differently from the muons produced in proton-proton collisions, it is shown that the final reconstruction performance is very good, not far from the performance expected from test beam studies and required for operation at the LHC.

The muon barrel system and its operating trigger conditions are described in section 2. After a brief discussion of the Monte Carlo simulation of cosmic ray data in section 3, the main features of the local muon reconstruction in the DT chambers are summarized in section 4. The results on hit reconstruction and local track segments are given in sections 5 and 6, respectively.

2 DT chamber setup and trigger conditions

A schematic view of CMS is shown in figure 1. As seen in the longitudinal view, the barrel part of the detector is divided in 5 wheels, named YB0, YB \pm 1, YB \pm 2 throughout this paper. All 250 DT chambers of the barrel muon system [7] were installed in the wheels and equipped for data taking at beginning of CRAFT. Two chambers were subsequently switched off for most of the data acquisition period due to hardware problems, which were solved by interventions carried out in the winter 2009 shutdown. Each wheel is divided into 12 sectors, each covering an azimuthal region of 30 degrees. Sectors are numbered anticlockwise, starting from the right-most vertical sector shown in figure 1 (bottom) in the direction of increasing azimuthal angle, ϕ . There are four layers of chambers (stations), named MB1-MB4 starting from the innermost one. In each station there is one DT chamber per sector, except in the uppermost (lowermost) sector, named sector 4 (sector 10), where the station MB4 is physically made of two DT chambers.

There is a vertical shaft leading from the cavern to the surface originally used for lowering parts of the CMS detector into the cavern. This shaft is located on the negative z side of the detector, and as a consequence, the cosmic rays flux was not uniform along the z coordinate of CMS, decreasing by about 20% when passing from wheel YB-2 to YB2.

A schematic layout of a DT chamber and of a DT cell are shown in figure 2. In each chamber there are 12 layers of contiguous drift tube cells grouped in three “superlayers” (SL) with 4

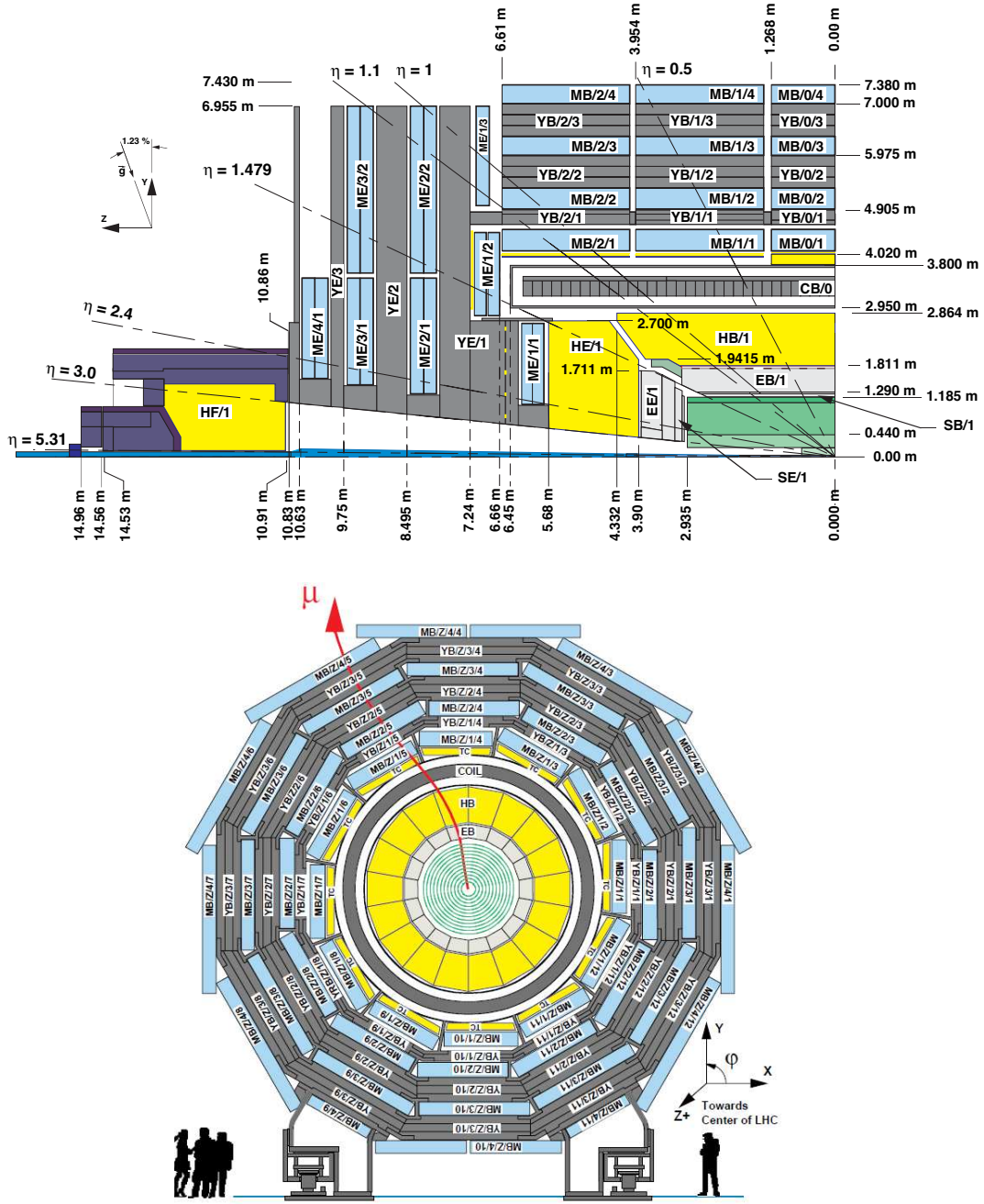


Figure 1. Schematic view of the CMS detector. Top: longitudinal view of one quarter of the detector. Bottom: transverse view at $z = 0$. The barrel muon detector elements are denoted as MBZ/N/S, where $Z = -2, \dots, +2$ is the barrel wheel number, $N = 1 \dots 4$ the station number and $S = 1 \dots 12$ the sector number. Similarly, the steel return yokes are denoted YBZ/N/S.

staggered layers each; the innermost and outermost SLs, labeled SL1 and SL3 in the figure, are dedicated to coordinate measurement in the CMS bending plane (r - ϕ plane), while in the central SL, labeled SL2, the hits are measured along the beam axis (r - z plane). The outermost stations,

named MB4, located outside the steel return yokes of the CMS magnet, have only the two SLs measuring the hit position in the r - ϕ plane. The distance between the anode wires of consecutive cells is 4.2 cm; the cells are separated by 1 mm thick aluminium I-beams glued between two 2.5 mm thick aluminium plates separating consecutive layers. Also visible are the aluminium strips, named “electrodes” in the figure, below and above the anode wire of the cell, which are needed to shape the electric field lines. This field shaping guarantees a good linearity of the cell behaviour over almost the entire drift volume [8]. The chambers are operated with an Ar/CO₂ (85/15%) gas mixture. The voltages applied to the electrodes are +3600 V for wires, +1800 V for strips, and –1200 V for cathodes. The electron drift velocity is about 54 $\mu\text{m/ns}$. The DT readout electronics is capable of recording multiple hits in the same cell, with a dead time of 150 ns between consecutive signals.

At the operating value of $B = 3.8$ T for the magnetic field inside the solenoid, typical values of the magnetic field inside the steel return yokes of the magnet structure, where the muon chambers are located, range between 1.2 and 1.8 T. In the active volume of the DT chambers, the residual magnetic field is generally small (below 0.2 T), except for the innermost chambers in the outermost wheels YB \pm 2.

The DT chamber Local Trigger [9] performs a rough track reconstruction within each SL and uniquely assigns the parent bunch crossing number to a track candidate. A Track Correlator processor associates track segments in the same chamber by combining the information from the SLs of the r - ϕ view, enhancing the angular resolution and providing a quality hierarchy of the trigger primitives. Up to two local trigger primitives are transmitted to the Regional Muon Trigger, which constitutes the following step of the level-1 muon trigger, running an algorithm called DT TrackFinder. This algorithm links the track primitives and forms muon candidates, assigning their angular coordinates and transverse momentum measurement. The DT local trigger was operating in all the sectors and wheels of the barrel muon system. After proper chamber synchronization within the same sector and between neighbouring sectors, the DT TrackFinder trigger provided a stable cosmic muon rate of about 240 Hz for the entire one month period of data taking [10]. It was operated with an open look-up table configuration requiring the coincidence of local triggers from at least two chambers in the same sector, with no requirements on the muon candidate direction and transverse momentum. The combination of the two chambers used correlated trigger candidates from the trigger processor in each station, which combines the trigger primitives between the chambers’ SLs in the r - ϕ bending plane [10].

3 Monte Carlo simulation of cosmic ray data

A simulation of the cosmic muon spectrum [11] has been used to compare the detector performance in the simulation to the data. About 20 million events with a muon momentum above 4 GeV/c, as defined on a cylindrical surface of 8 m radius co-axial with the CMS z -axis, were generated and processed through the full CMS simulation and reconstruction chain. The magnetic field inside the CMS solenoid was set to $B = 3.8$ T. The muon crossing time at the top of the CMS detector was generated according to a flat distribution within a ± 12.5 ns time window, to replicate the random arrival time of the muon in a bunch crossing window (25 ns) of the trigger. The time signals that constitute the Time-to-Digital Converters (TDCs) raw data were generated by the digitization

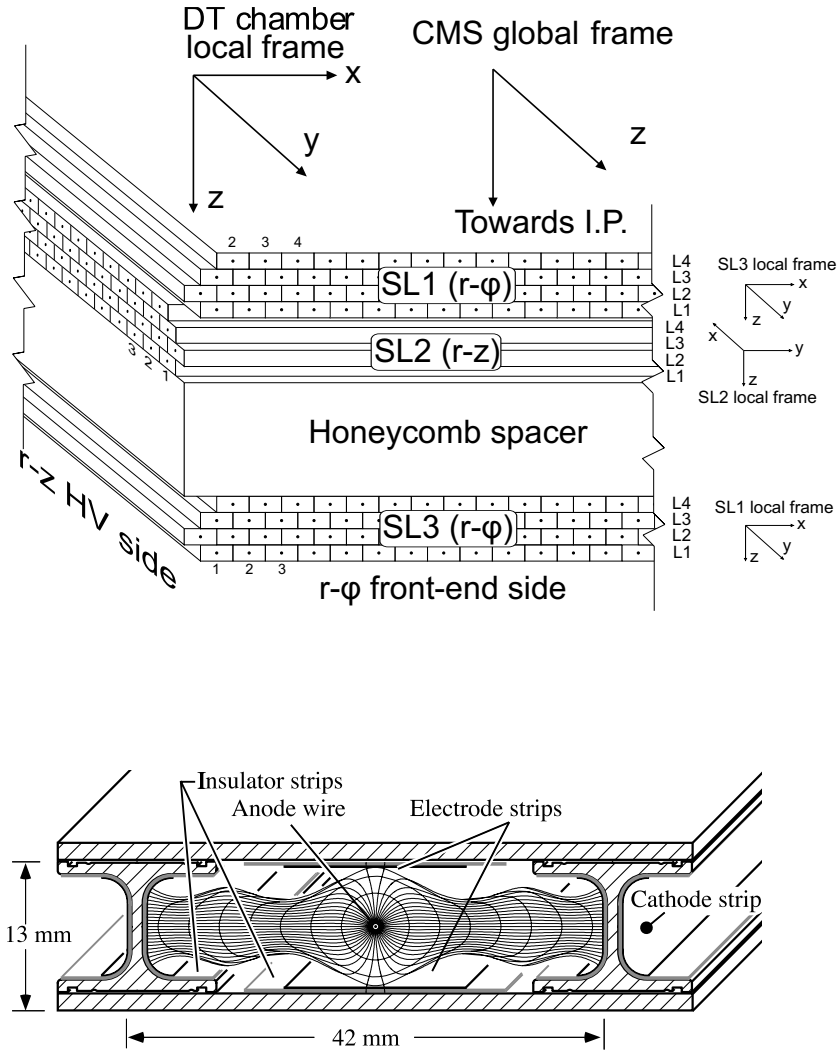


Figure 2. Top: schematic layout of a DT chamber. The distance between the innermost and outermost superlayer (SL) in the chamber is about 25 cm. The SL1 and SL3 superlayers measure the $r-\phi$ coordinate in the bending plane of CMS; the SL2 superlayer measures the z coordinate, along the direction parallel to the beam (perpendicular to the plane of the figure). Bottom: layout of a DT cell, showing the electric field lines in the gas volume.

algorithm based on the parameterization of the DT cell response described in ref. [12] and tuned on test beam data, taking into account the muon time of flight from chamber to chamber.

A realistic representation of misalignments based on the analysis of CRAFT data [13] was implemented in the CMS detector simulation. The CMS alignment strategy combines precise survey and photogrammetry information, measurements from an optical based muon alignment system [14], and the result of the alignment procedures based on muon tracks [13]. A complete alignment of all muon chambers was not available for CRAFT. For the internal geometry of the

DT chambers, which is relevant for the local reconstruction of the muon tracks, the spread of the measurements of the layer relative positions measured during chamber construction and of the photogrammetry measurements made on reflective targets on the exterior of the superlayers were taken into account in the geometrical database of the detector. In the simulation, typical RMS deviations from the ideal detector geometry are taken to be $100\text{ }\mu\text{m}$, with $30\text{--}40\text{ }\mu\text{m}$ systematical uncertainty for the layer position, and about $200\text{ }\mu\text{m}$ for the superlayer positions inside the chamber. The positions of the muon chambers in the global CMS reference system were misaligned with a 2 mm Gaussian smearing in x , 4 mm in y and z , reflecting the initial uncertainty expected from the available photogrammetry measurements, taken with the CMS detector open. The orientations of the chambers in $r-\phi$ and $r-z$ planes were smeared by 2 mrad.

4 Local reconstruction of muon tracks

In the first stage of the local reconstruction, the hits in each DT cell are reconstructed starting from the measured time associated to them, as recorded by the TDCs. The electron drift time, t_{drift} , is computed from the TDC raw data by performing the following operations:

- subtraction of the inter-channel synchronization constants, T_0 s, which correct for different signal path lengths of readout electronics in the chamber front-end. The T_0 s are measured using electronic test pulse signals [15].
- subtraction of the “time-pedestal”, t_{trig} , computed at the superlayer level in each chamber. The quantity t_{trig} accounts for the time latency of the Level-1 trigger and the time of flight of the muon to the chamber. It is computed by a calibration procedure that fits the rising edge of the distribution of the TDC recorded times for all the cells in the superlayer, as described in detail in ref. [15].

A typical distribution is shown in figure 3 for real and simulated data, after the measured T_0 ’s have been subtracted cell-by-cell. The peak at the beginning of the time distribution is due to non-linear effects in the avalanche region very near (a few wire diameters wide) the anode wire, and to the occurrence of δ -ray electrons which pass closer the anode wire than the muon track. The tail in the real data after the “time-box” distribution (i.e. for TDC time greater than 2800 ns which, for the specific superlayer shown in the figure, corresponds to the maximum drift length in the cell) is due to “feed-back” electrons. These are electrons extracted either from the cell I-beam or from the aluminium strips (see figure 2) by photons produced in the cascade process initiated by the primary electrons very near the anode wire (these photons are not further considered in the simulation). The arrival time of the signal associated with these feed-back electrons thus exceeds the maximum drift time in a cell. The stability of the calibration results and their dependence on trigger conditions and chamber locations is discussed in ref. [16].

Hits with $t_{\text{drift}} < -3\text{ ns}$ are discarded, while hits having $-3 < t_{\text{drift}} < 0\text{ ns}$ are retained and assigned the position $x = 0$ in the local reference frame of the cell, corresponding to the anode wire position. The conversion from time measurements to hit positions in a DT cell [17], leading to one-dimensional reconstructed hits, or “rechits”, was performed assuming a constant effective drift velocity in the whole chamber volume, independent of track position and inclination. This

assumption is justified for all chambers except the innermost stations, MB1 n ($n = 1 \dots 12$), of those mounted on the YB2 and YB-2 wheels [16]. More sophisticated algorithms [17] based on a detailed parametrization of the DT cell behaviour, developed using simulated data, are currently under study. For the purposes of the present studies, however, including the MB1 chambers in the outermost wheels, the current algorithm is adequate (once the correct average value of the drift velocity in these chambers is properly taken into account), as will be shown in section 5.

For each TDC signal there are two possible rechits due to the left-right ambiguity on the position with respect to the anode wire inside the cell. This ambiguity is resolved at the track segment building stage [17] by the local pattern recognition algorithm that takes the rechits as input, thanks to the staggered structure of the cells in the chamber SLs as shown in figure 2. The pattern recognition is initiated by considering all possible pairs of hits (seeds) in different layers, starting from the most separated hits in the chamber. For each seed, additional hits are searched for in all layers and included in the segment candidate if they are compatible with the extrapolation from the seed within a loose requirement (2 mm). Segment candidates are built by performing a straight-line fit to the associated hits and sorted on the basis of their total number of hits and χ^2 , defined as the sum of the squares of the hit residuals divided by the hit position error, normalized to the number of degrees of freedom. The sagitta of the muon track in the (generally small) residual magnetic field in the chamber volume is negligible. For each seed, only the segment candidate with the maximum number of hits is considered; among the candidates with the same number of hits, the one with best χ^2 is selected. Segments with at least three hits and $\chi^2/NDOF < 20$ are finally retained.

The pattern recognition is performed independently in the r - ϕ and r - z SLs of each chamber to deliver the so-called 2-dimensional (2D) track segments in both views. The 2D segments are then paired using all possible combinations to form 4-dimensional (4D) segments in the chamber, carrying 3-dimensional spatial information and the fitted value of the arrival time of the muon in the chamber (see next section). The arrival time of the TDC signal determining the position in a given direction is corrected for the signal propagation time along the cell wire, using the position information of the associated hits measured in the orthogonal view of the chamber, and the rechit position is updated in the 4D segment accordingly. The 4D segments are used as input to the subsequent stage of the global muon reconstruction that links the information from different muon stations and from the tracker detector to fit a unique track. The reconstruction used the standard CMS reconstruction code that takes into account the alignment corrections obtained from the knowledge of the internal structure of most chambers, but not yet the complete information of the chambers' position in the CMS structure.

5 Reconstructed hits in DT chambers

One-dimensional reconstructed hits in the DT cell are the basic objects from which the muon track reconstruction is initiated. This section summarizes the main results concerning the hit resolution and reconstruction efficiency.

5.1 Spatial resolution

The one-dimensional hits are first determined assuming a fixed arrival time in the chamber of the cosmic muon, $t_0 = 0$, inside the 25 ns wide window associated with the L1 trigger. At this stage

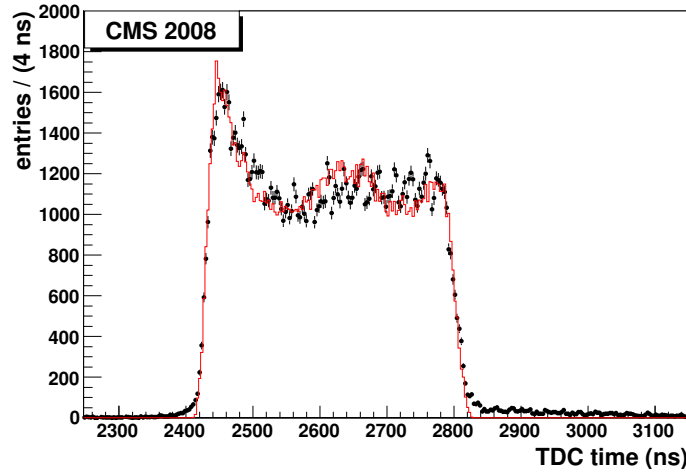


Figure 3. Distribution of the signal arrival time in CRAFT (points) and simulated data (full line histogram). The arrival time in all the cells from a single superlayer in a chamber are shown, after the cell-by-cell equalization based on electronic test-pulse calibration.

the hit resolution is about $660 \mu\text{m}$, largely dominated by the uncertainty on t_0 . Once the local pattern recognition is performed and local segments are built, a re-fit is performed treating t_0 as a free parameter, recomputing the hit positions and the final segment position and direction. At this final stage of the local reconstruction, the resolution is about $260 \mu\text{m}$, in good agreement with the requirements for collision data [7] and the results from test beam measurements [8].

A measure of hit resolution is provided by the residuals of the hit position with respect to the predicted position in the layer obtained from the segments, reconstructed excluding the hit under study from the fit. The distribution of the residuals in the r - ϕ SL's with respect to the position obtained from the segment extrapolation is shown in figure 4, for the first stage of the hit reconstruction. The data are shown for the four stations of sector 4 in the central wheel of the barrel detector. Only segments with more than 6 hits used in the fit were considered. The full line histograms shown in the left plots in the figure correspond to the hit residual distributions from “off-time” events, i.e., events triggered with a bunch crossing identification provided by the local trigger of the chamber differing by ± 1 (in 25 ns units) from the one occurring more frequently. As expected, for this population of events the spread of the residuals is significantly larger, since the subtracted time pedestal computed by the calibration procedure is shifted on average by ± 25 ns with respect to the muon arrival time. The double peak structure for these events reflects the staggering of the DT cells between consecutive layers: hits occurring on the half-cell volume on the left side of the anode wire have a bias opposite with respect to hits occurring in the half-cell volume on the right side.

In the right plots of figure 4 the distribution of the residuals is shown both for real and simulated data for “in-time” events, i.e., for events triggered with the most frequent bunch crossing identification in the chamber. A single Gaussian fit to the residual distributions, shown by the curve superimposed to the data point, gives $\sigma_{\text{res}} = 620 \mu\text{m}$. To have an estimation of the hit resolution at this stage, this value must be corrected for the segment extrapolation error, which at this

reconstruction stage is on average $\sigma_{\text{extrap}} = 320 \mu\text{m}$ (slightly dependent on the layer position of the hit under test). The observed single hit resolution is thus:

$$\sigma_{\text{hit}} = [\sigma_{\text{res}}^2 - \sigma_{\text{extrap}}^2]^{1/2} = 530 \mu\text{m}. \quad (5.1)$$

The pedestal-subtracted time recorded by the TDC is the sum of the electron drift time (ranging from 0 to a maximum of about 380 ns for muon tracks passing at the DT cell boundary [4]), the random arrival time t_0 of the muon in the trigger window and the time of the signal propagation along the anode wire. This last effect can be taken into account once the segment pattern recognition is performed in the orthogonal superlayer and the hit position along the wire is determined. The expected hit resolution is then:

$$\sigma_{\text{hit}} = [\sigma_{\text{cell}}^2 + \sigma_{t_0}^2 + \sigma_{\text{prop}}^2]^{1/2} = 470 \mu\text{m} \quad (5.2)$$

roughly consistent with the observed value. In the expression above, $\sigma_{\text{cell}} = 200 \mu\text{m}$ is the intrinsic position resolution of the DT cell as measured with muon test beam [18] and $\sigma_{t_0} = (25 \text{ ns} / \sqrt{12}) \cdot v_{\text{drift}} = 390 \mu\text{m}$ is the contribution due to the uncertainty of the muon arrival time for an average electron drift velocity $v_{\text{drift}} = 54 \mu\text{m/ns}$ [18]. Finally $\sigma_{\text{prop}} = v_{\text{drift}} \cdot \sigma_t = 160 \mu\text{m}$ is the uncertainty due to the signal propagation along the anode wire, where $\sigma_t = (l / \sqrt{12}) / v_{\text{prop}}$, $v_{\text{prop}} = 0.244 \text{ m/ns}$ is the signal propagation velocity [19] and $l = 2.5 \text{ m}$ is the anode wire length. The corrections with respect to the ideal detector geometry for the layer misalignments inside the chambers [13] have been included in the reconstruction. The contribution to the observed hit resolution from the remaining uncertainty (of the order of 30-40 μm) on this corrections is negligible.

The distribution of the hit resolution, obtained using eq. (5.1) from the RMS values of the Gaussian function fit to the hit residuals, is shown in figure 5. The average value of the distribution obtained for 246 chambers is 660 μm with an RMS of about 200 μm . In addition to the two chambers completely switched off, there were two chambers in sector 8 of YB1 and YB-1 respectively having the innermost r - ϕ SL switched off (cfr. figure 11), for which the hit resolution study was not performed. It is worth noting that the tail in the distribution comes from the chambers in the most inclined sectors with respect to the horizontal direction. In particular, the worst performance is obtained in the chambers of the vertical sectors 1 and 7 (corresponding to the shaded entries shown in the histogram), where the average direction of the triggered cosmic muons with respect to the chamber normal axis is larger than 50 degrees. In this condition, which is very far from the one expected for prompt muons originating in pp collisions at the LHC, the t_{trig} determination has larger uncertainties and the effects due to cell non-linearity become important.

After the local pattern recognition, the arrival time of the muon, t_0 , can be treated as a free parameter in a refit of the segment that determines the final segment position and direction [4]. Typical distributions of the fitted muon arrival time in the chambers of sector 4 are shown in figure 6, for all events triggered by the local trigger, and separately for bunch crossings differing from the most common by one. The local trigger assigns the candidate track to a given bunch crossing time window, defined with 25 ns granularity. The distributions of the bunch crossing identification number in all the chambers of the sector are also shown in figure 6. Although the number is arbitrary, it is evident that the tails are dominated by events triggered at the bunch crossing differing by ± 1 from the most commonly identified crossing of 12. The differences between the

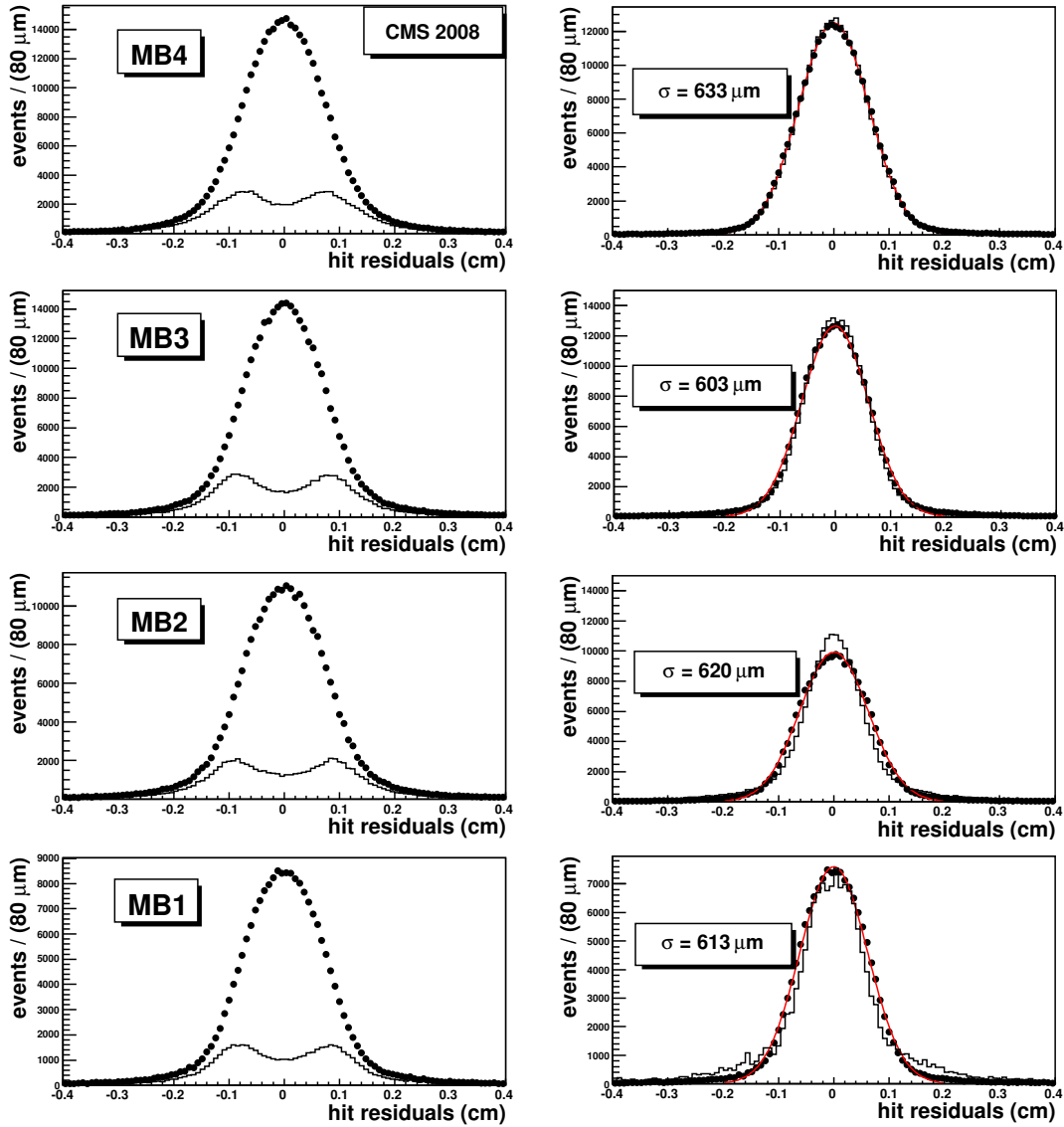


Figure 4. Hit residuals in DT muon chambers of YB0, sector 4, at the first stage of the hit reconstruction. Left column plots: all events; the full line histograms show the hit residuals for the events with bunch crossing identification in the chamber different from the most frequent one. Right column: events with the most frequent bunch crossing identification; real data: points, simulated data: full histogram. The curves show the result of a fit to the data using a Gaussian function. The fitted RMS values are listed.

distributions of the bunch crossing identification shown for different chambers in the lowest right plot are due to the imperfect fine tuning of the synchronization of the local trigger devices of the chambers [20]. In this sector, for MB1 and MB2 chambers, the population of events with bunch crossing 11 is practically absent, as a consequence of the muon time of flight, which enhances the probability to have in these stations a bunch crossing identification number shifted by +1 with respect to the bunch crossing number assigned by MB3 and MB4. The differences between the fitted arrival times in consecutive chambers are also shown in the figure. It must be stressed that the

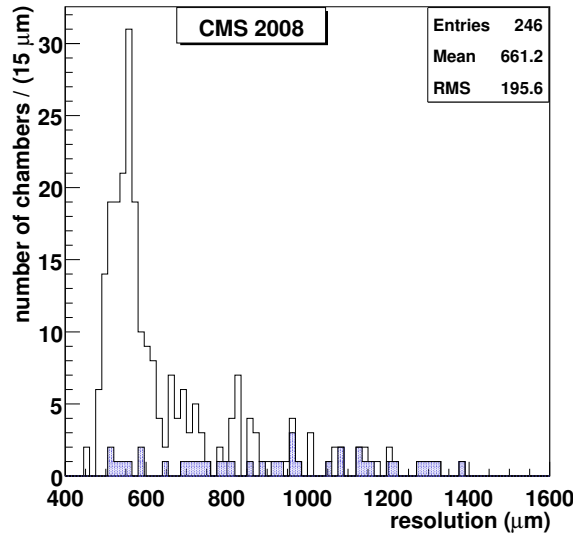


Figure 5. Distribution of the hit resolution computed using eq. (5.1) from the RMS values of the Gaussian function fitted to the reconstructed hit residuals in all DT chambers, obtained at the first stage of the local reconstruction. The dark entries are from chambers in the vertical sectors. Four chambers are not included in the plot due to powering problems.

time pedestal calibration procedure mentioned above is defined by taking into account the muon time of flight between them. The average values of the distribution of the time differences between consecutive chambers are thus expected to be zero.

The distribution of the hit residuals after the t_0 refit is shown in figure 7 for sector 4 of the external wheel YB–2. In this wheel (as well as in wheel YB2), the residual magnetic field in the chambers volume has the largest variation along the chamber’s length, reaching the highest values (up to 0.8 T for the radial component in the MB1 stations [7]). This variation does not affect significantly the average hit resolution observed in the chamber, once the corresponding average change of the effective electron drift velocity (about 2% for MB1 chambers [16]) is taken into account in the reconstruction. As for the distributions shown in figure 4, the residuals are computed with respect to the extrapolated position from the segment, obtained excluding the hit under study. The residuals are shown for all the triggered events. Plots of the hit residuals vs. the distance to the anode wire in the DT cells are shown in figure 8, displaying the good uniformity of the cell behaviour in the whole drift volume. Moreover, the approximate straight line behaviour of the mean value of the residual distribution in each bin demonstrates that non-linear effects are smaller than $100 \mu\text{m}$. This is in agreement with accurate studies performed on dedicated test beam data, that show deviations from linearity not larger than $60 \mu\text{m}$ [18]. Although the distributions of hit residuals have width significantly narrower than the corresponding distributions obtained before the t_0 fit, they still have rather large tails. These are due to displaced hits from δ -rays, originally included in the segment by the pattern recognition algorithm. It is worth remembering here that the algorithm was run with a loose criterion to include a hit in the segment, in order to cope with the initial uncertainty on the hit position dominated by the t_0 jitter. The distributions of hit residuals

were fitted with a sum of two Gaussian functions, constrained to have the same mean values. As seen in figure 7, the narrower Gaussian gives $\sigma \approx 280 \mu\text{m}$, accounting for about 80% of the total population, while the wider Gaussian has $\sigma \approx 1 \text{ mm}$.

The distribution of the hit resolution, computed using eq. (5.1) from the RMS values of the narrower Gaussian function fitted to the reconstructed hit residuals in all the DT chambers, is shown in figure 9. The value of the extrapolation error used in eq. (5.1) is $\sigma_{\text{extrap}} = 140 \mu\text{m}$. For most of the chambers, the resolution is approximately $260 \mu\text{m}$. Again, the tail at large values comes from chambers in the sectors most inclined with respect to the horizontal direction. The shaded entries in the histogram are from vertical chambers.

5.2 Hit reconstruction efficiency

The hit reconstruction efficiency is measured by looking for hits in a given layer after extrapolating the local segment fit to that layer. The extrapolation is done with hits on the segment after excluding in the reconstruction the hits in the layer under consideration. Figure 10 shows the efficiency as a function of the predicted hit position in the cell for MB1 stations (data from all the cells from all the chambers of a given type are combined in the plot). The efficiency is greater than 98% over a large part of the drift volume. Similar behaviour is observed for the MB2–4 stations. The observed small inefficiency near the anode wire ($x = 0$ in the plots) is due to the pedestal subtraction procedure described in section 4 and is well reproduced by the simulation. However, near the cell boundaries the efficiency is overestimated by the simulation in the last millimeter of the cell volume (corresponding to 5% of the total sensitive volume). No significant difference between the data at $B = 0 \text{ T}$ and $B = 3.8 \text{ T}$ is observed. The noise effect is negligible in this plot because the number of noisy cells having an occupancy larger than 1% in the recorded data amounts to less than 0.1% of the total number of DT cells. A detailed study of noise rates in the DT system can be found in ref. [15].

Figure 11 summarizes the results for the hit efficiency in all the layers of the DT chambers, averaged over all the cells of the considered layer. The efficiency is higher than 95% almost everywhere in the barrel detector, with a small decrease in the vertical sectors.

6 Reconstructed track segments in DT chambers

The second stage of the local track reconstruction described in section 3 provides “2D” and “4D” track segments, which are studied in detail in this section.

6.1 Multiplicity of associated hits and track segment efficiency

Reconstructed hits are associated to 2D track segments built independently in the r - ϕ and r - z planes, as described in section 3. Collections of 4D track segments are then built considering all possible combinations of 2D r - ϕ and r - z segments in each chamber. The distributions of hit multiplicities for all reconstructed 4D track segments are shown in figure 12 for each DT station in the horizontal sectors of YB1 separately. The distributions are peaked, as expected, at the total number of layers in the chamber (8 in MB4 and 12 in the other stations), although the Monte Carlo simulation predicts a slightly larger average multiplicity. Track segments that have a large incident angle and pass near the boundary between neighbouring drift cells may have more than one associated hit in a given layer, thus resulting in a hit multiplicity larger than the number of layers in

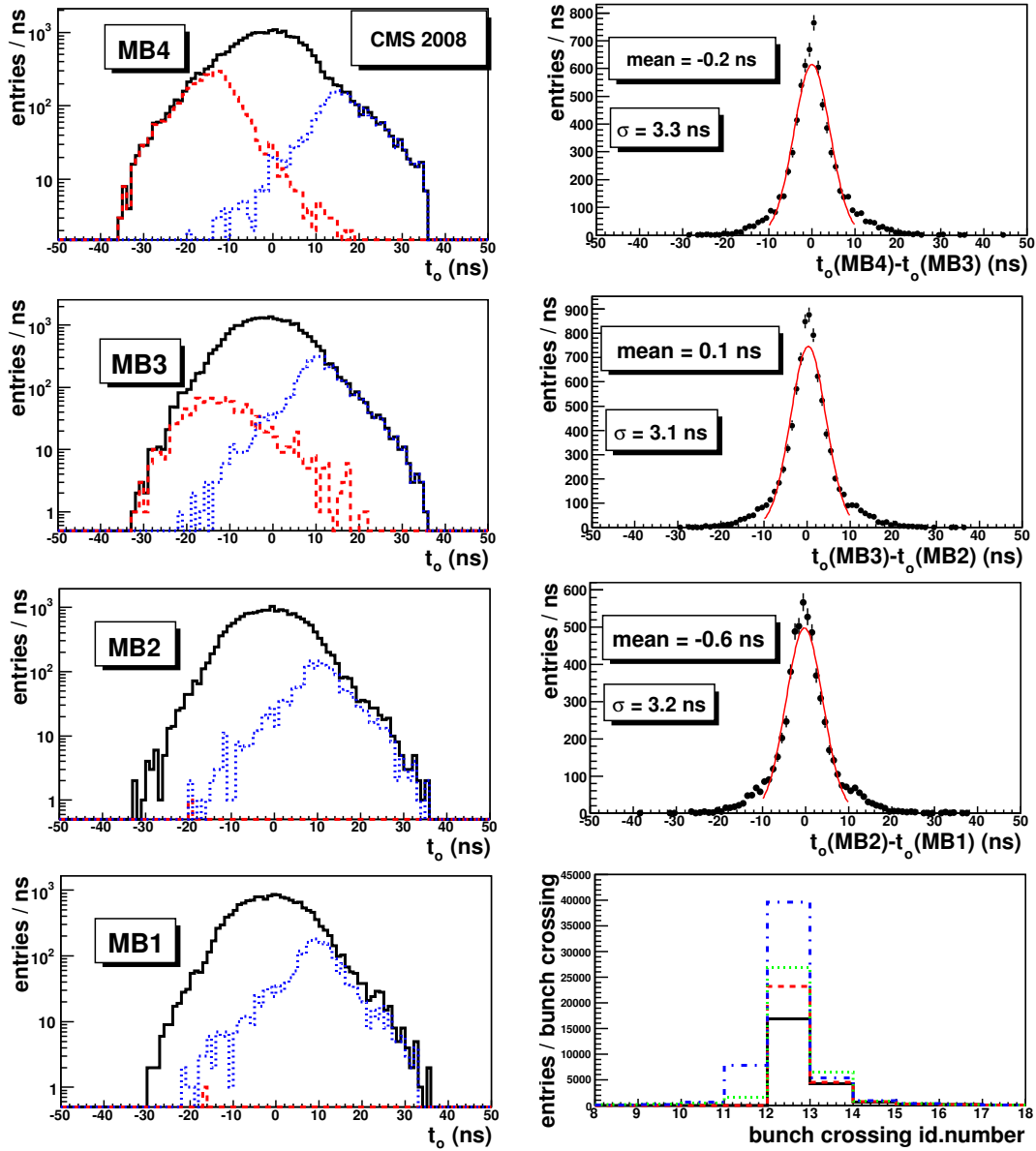


Figure 6. Left column: distributions of the fitted arrival times of the muon in the chambers of sector 4 in YB-1. The full line histograms refer to all events triggered by the local trigger. The dotted (dashed) line histograms refer to events with bunch crossing identification = +1 (-1) with respect to the most frequent bunch crossing (12) provided by the local trigger in each chamber [9]. Three upper right plots: distributions of the difference of the t_0 values between two consecutive stations. The curves show the result of a Gaussian fit over the range [-10,+10] ns. The fit results are given to provide a rough measure of the mean and RMS of the core of the distribution. Bottom right plot: distributions of the bunch crossing identification in the four chambers of the sector (full line histogram: MB1; dashed line: MB2; dotted line: MB3; dashed-dotted line: MB4).

the station. The distribution of the segment incident angle with respect to the vertical axis in the bending plane of CMS, also shown in figure 12, is well reproduced by the simulation. The observed increase of the spread around the normal direction when passing from MB4 to MB1, i.e. from the

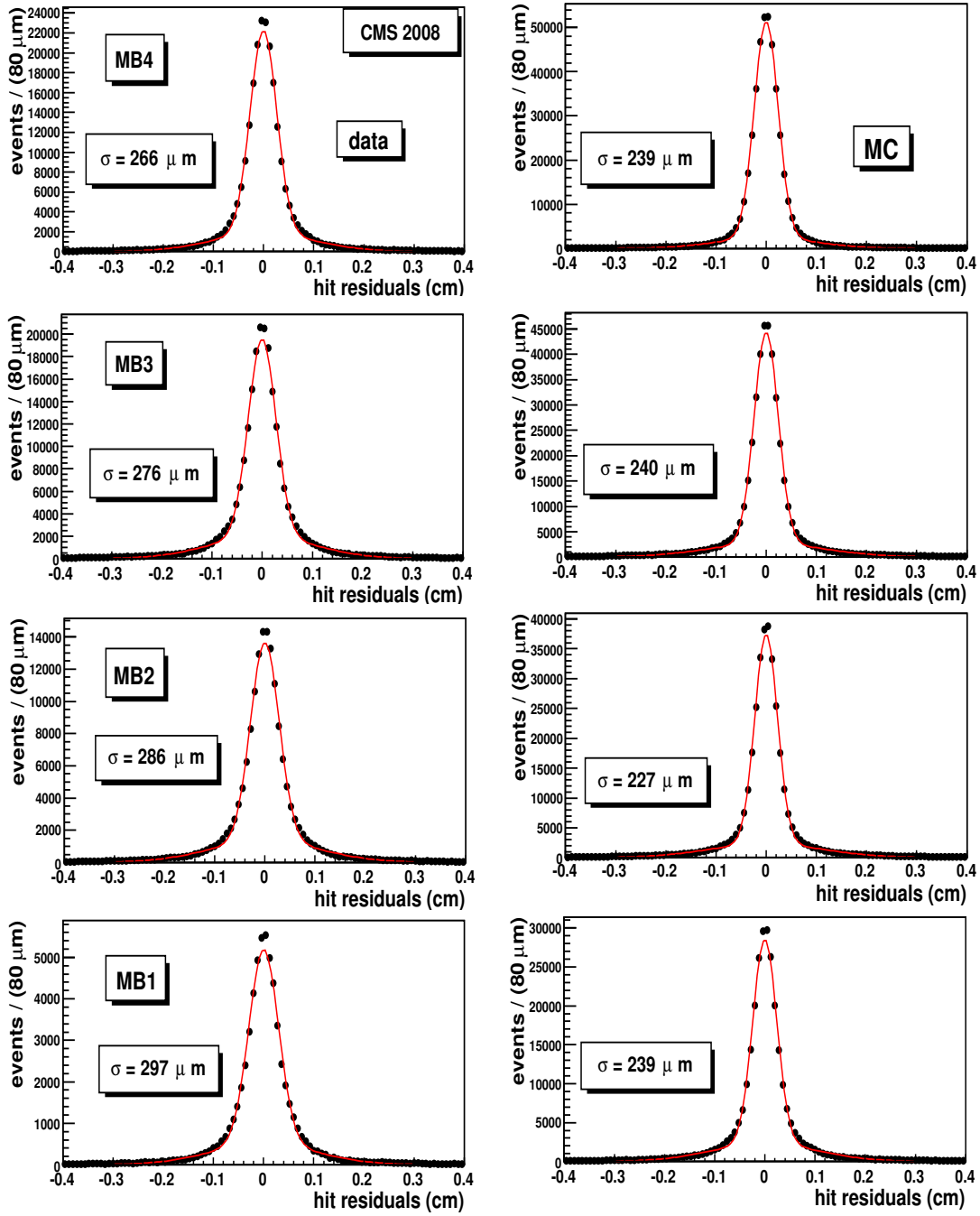


Figure 7. Hit residuals in DT muon chambers of YB-2, sector 4 after t_0 segment refit. Left column: data; right column: simulation. The curves show the result of a fit to the data using a double Gaussian function. The fitted RMS values of the narrower Gaussian function are listed.

outer to inner stations (from top to bottom plots in the figure), is due to the opposite bending effects of the magnetic field in the steel yokes on positive and negative muons.

The difference between data and simulation in the hit multiplicity distributions is due to the discrepancy in the hit reconstruction efficiency observed near the I-beams separating the DT cells

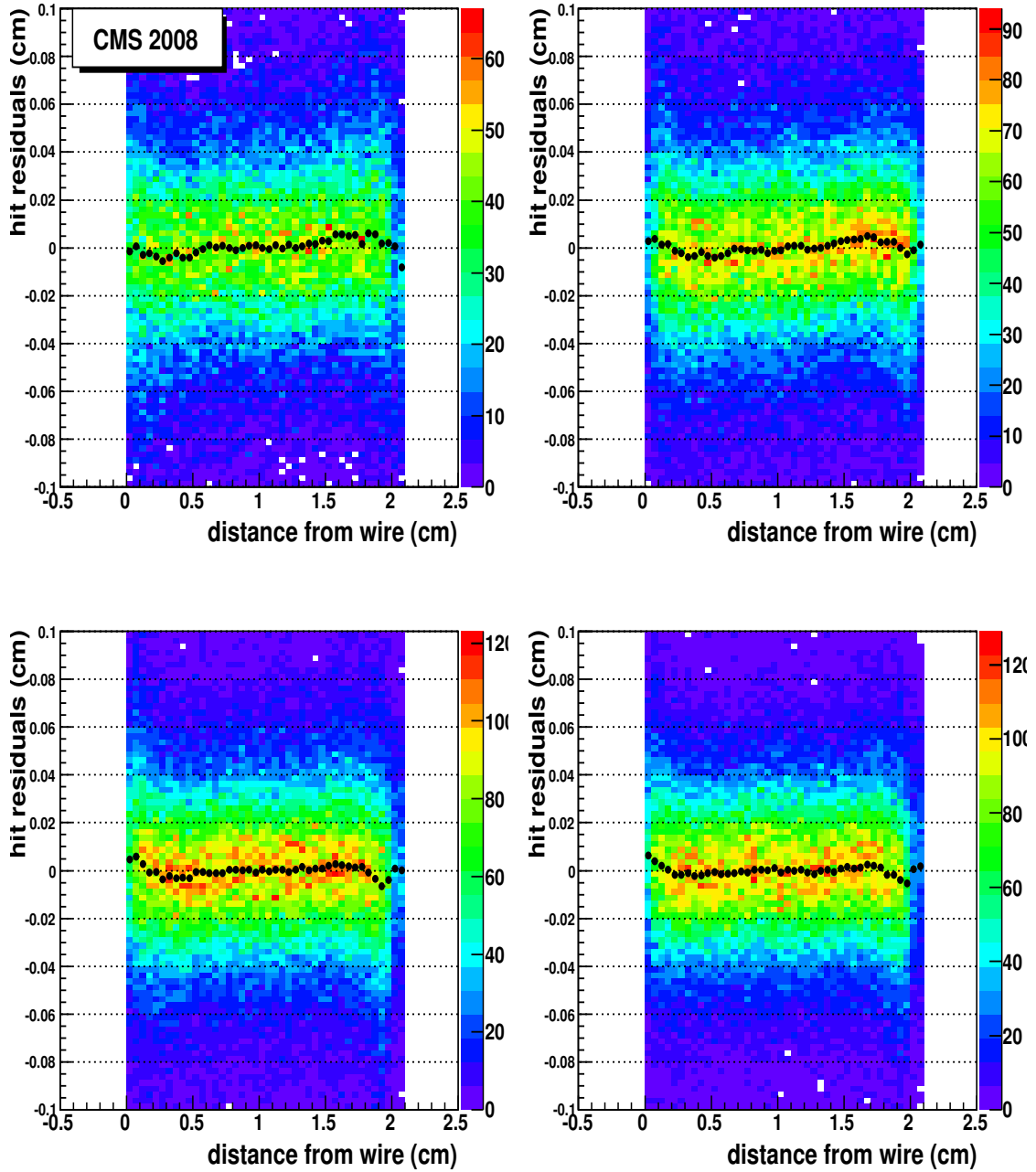


Figure 8. Plot of residuals vs hit position in a DT cell, for the chambers of YB–2, sector 4; the plot profile is shown by the points. Top plots: MB1 (left) and MB2 (right). Bottom plots: MB3 (left) and MB4 (right).

(see figure 10) and additional small discrepancies, which sum up independently in the different layers used in the segment reconstruction. As an example of such small discrepancies, figure 13 shows the efficiency for hit reconstruction and association to the muon track, in a region extending approximately over four cells in two consecutive layers of an r - ϕ superlayer of the MB2 chamber in

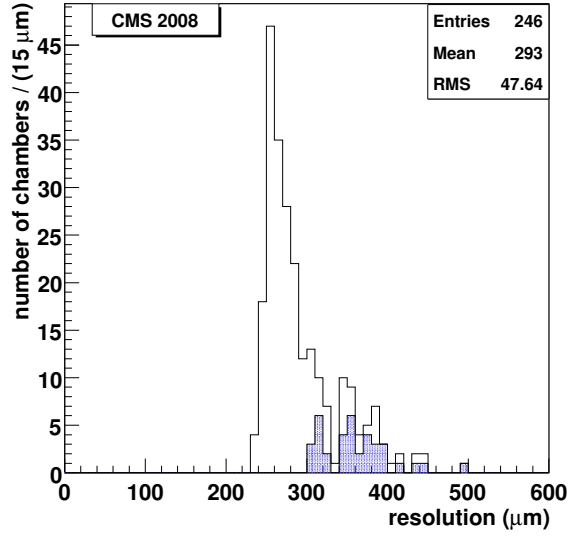


Figure 9. Distribution of the RMS values of the narrower Gaussian curve fitted to the reconstructed hit residuals in all DT chambers, after t_0 segment refit. The plotted values have been corrected for the track extrapolation error. The dark entries are from chambers in the vertical sectors.

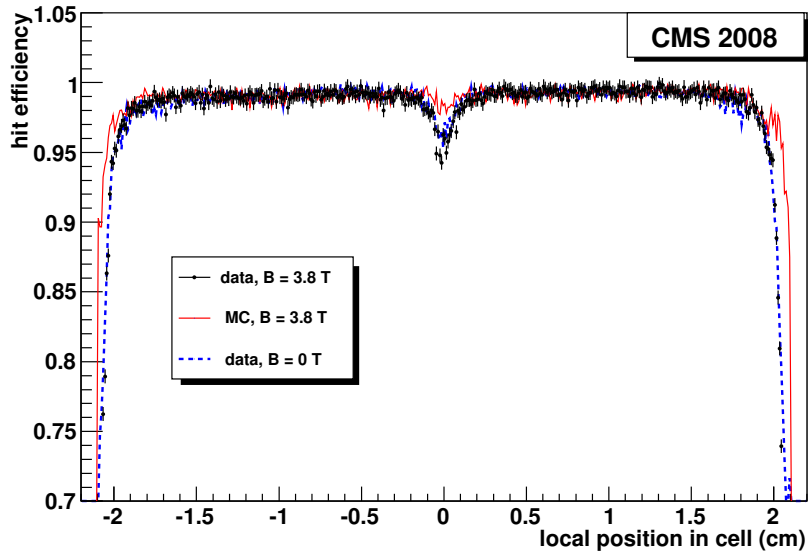


Figure 10. Efficiency to have reconstructed a hit in a cell crossed by a cosmic muon, as a function of the predicted muon position in the cell, for the MB1 stations. The $x = 0$ position corresponds to the location of the anode wire in the cell.

the top sector (sector 4) of YB0. As can be expected, the discrepancy between data and simulation is larger near the cell boundaries (0, 4.2, 8.4 . . . cm in the first layer shown, staggered by half a cell between consecutive layers). In addition, a decrease of the efficiency can be due to the presence

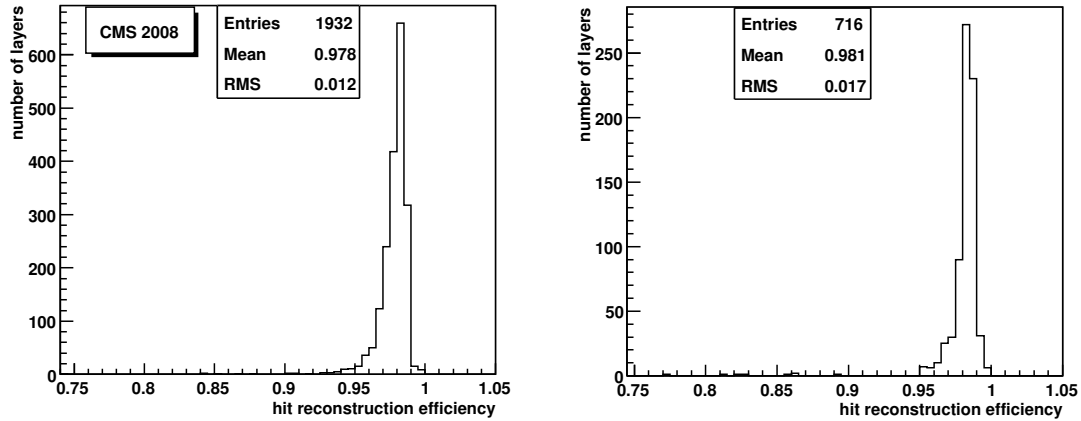


Figure 11. Average of the reconstructed hit efficiency in the layers of the Muon Barrel DT chambers. Left: r - ϕ superlayers; right: r - z superlayers.

of a noisy cell, as is the case for the fourth cell in the upper plot. A pulse due to noise can indeed mask the hit produced by the muon, which is therefore lost. Since the number of noisy DT channels is at the level of a few per mille [15], the overall effect on the multiplicity distributions shown in figure 12 is however negligible. A discrepancy at a few percent level is also visible for distances larger than about 1 cm from the anode wires (located at 2.1, 6.3 ... cm in the upper plot), due to non-linear drift effects. Finally, the inefficiencies observed very near the anode wires are in general small, especially in horizontal chambers like the one shown in figure 13, for which the time pedestal determination has a small uncertainty.

The efficiency of reconstructed hit association is also affected by the occurrence of δ -ray electrons originating in the gas volume and/or in the mechanical structure of the chambers. If these electrons pass closer to the anode wire of the cell than the original muon, they mask the muon signal if it arrives within the electronics dead time of 150 ns. Figure 14 shows the distribution of the difference between the distance from the cell anode wire of the first hit recorded (independently from its association to the muon track segment) and the distance of the position of the track extrapolation. The population at large values of the distance difference is due to the δ -ray hits that are not associated to the track segment. The tail at positive values of the difference (extended to values bigger than the half-cell dimension to show the population from neighbouring cells in the same layer) is due to events with a δ -ray, where the muon hit goes undetected. The data and simulation distributions show a reasonably good agreement, both in the absolute yield of δ -rays and in the asymmetry of the distribution, with a slight underestimation of the effect in the simulated data. The shoulder seen at about 0.8 cm for $B = 0$ T data is due to signals from feed-back electrons (see section 4) extracted from the electrode strip below the anode wire in the cell. This effect is almost invisible in the $B = 3.8$ T data, due to the tilt of the electron drift paths which makes the detection of these electrons less efficient. Returning to figure 12, the difference of about 15% seen in figure 12 between real and simulated data in the fraction of segments having 12 associated hits (8 in MB4) is understood as mainly due to an average difference of about 1% in the hit reconstruction and association efficiency, concentrated in the part of the DT cell farther from the anode wire.

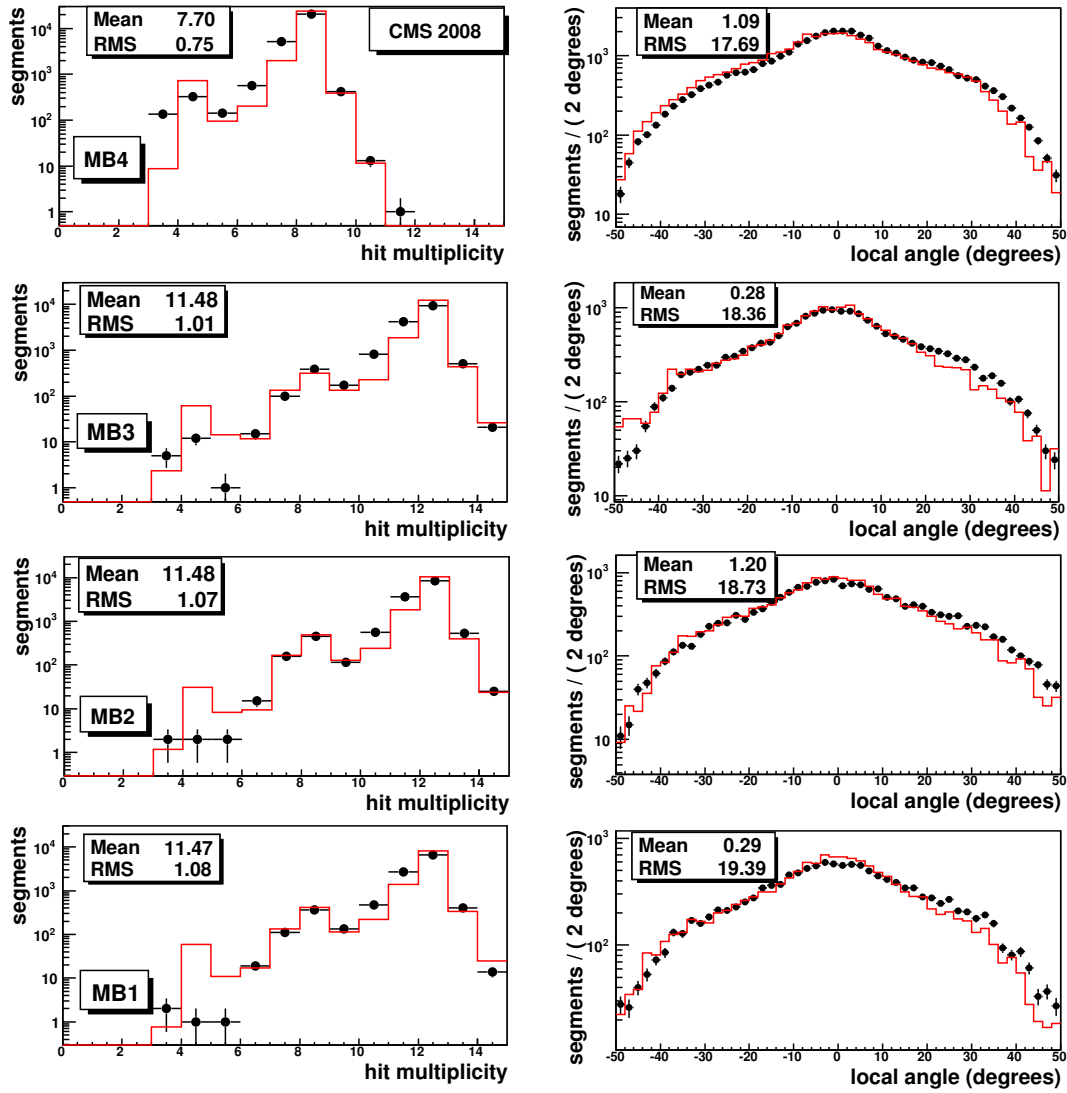


Figure 12. Left plots: multiplicity of associated hits in reconstructed 4D segments in YB+1, sector 4. Right plots: segment direction with respect to the vertical axis. Real data (points) and simulated data (solid line histogram) are shown in both sets of plots.

The evaluation of the segment reconstruction efficiency is performed using muon tracks reconstructed in the silicon tracker independently of the muon chambers. Distributions of the residuals between the reconstructed 2D r - ϕ segment intersection with the first layer plane in MB1 and the extrapolated tracker track position to the same plane for the muons in four different momentum ranges (as measured by the inner tracker system) are shown in figure 15. Similar distributions are observed for chambers MB2-MB4, with slightly increasing RMS values when going from the innermost to the outermost stations (e.g., RMS = 8.4 cm in MB2 and RMS = 10.7 cm in MB4 for muons with p_T in the [45–80] GeV/c range). The width of the distributions is dominated by the effect of multiple scattering in the calorimeters and in the steel return yokes of the magnet. It decreases at larger momentum, with a behaviour well reproduced by the simulated data. The small

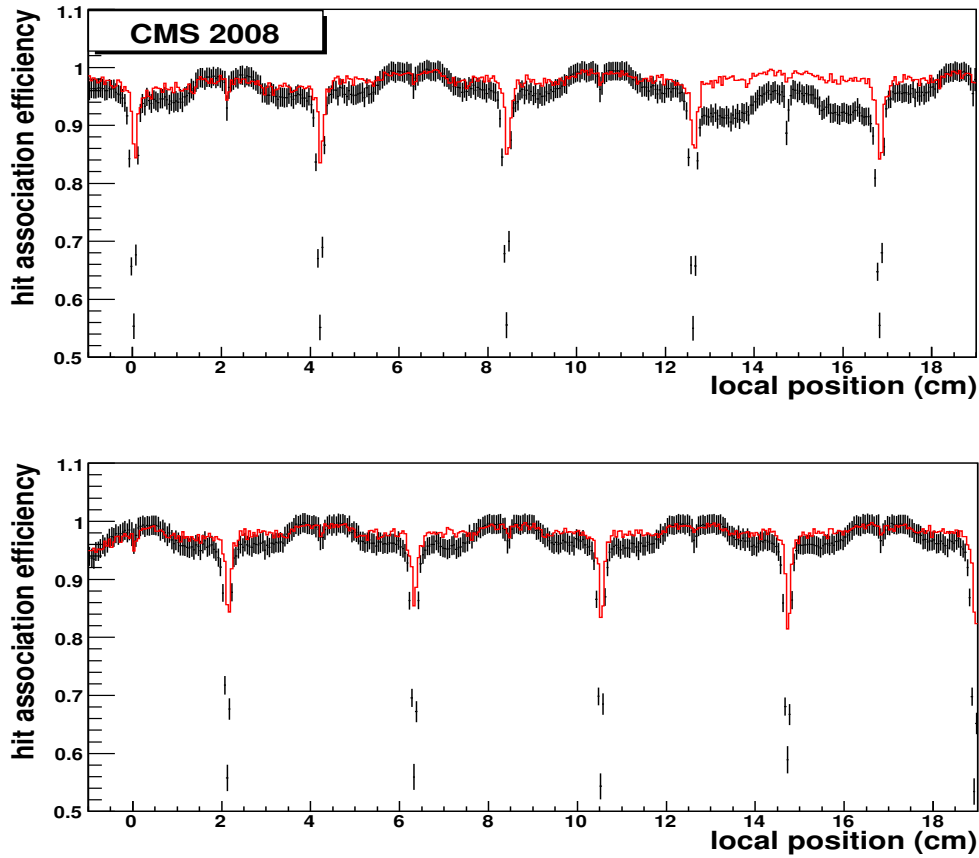


Figure 13. Efficiency for hit reconstruction and association to the muon track segment as a function of the predicted muon position in layer one (top) and layer two (bottom) of one SL in the MB2 station of sector 4 in YB0. A region corresponding approximately to four DT cells in each layer is shown. Points: data; full line histogram: simulation. Note the suppressed zero of the vertical axis.

discrepancy at large distance values, increasing with the momentum of the muon, is due to fluctuations in the muon energy loss which are slightly underestimated in the simulation. To measure the segment reconstruction efficiency, only muons with $p_T > 30 \text{ GeV}/c$ were considered. A window of 20 cm around the predicted position was used to accept a segment candidate. To ensure a reliable extrapolation from the tracker tracks, when computing the efficiency for a given chamber MB n , the extrapolation of the track to station MB($n+1$) (exceptionally MB3 when considering the efficiency of MB4 chambers) was required to be confirmed by a DT segment reconstructed with at least six associated hits also in this station MB($n+1$), within the same acceptance window as defined above. To avoid bias in the efficiency determination due to the trigger, in the selection for the efficiency computation of chamber MB n it was required that the event have high-quality local triggers delivering the same bunch crossing identification in at least two chambers in the same sector, excluding the chamber under study. This procedure guarantees that the events were triggered independently from the trigger response of the local trigger device of the considered chamber. The segment reconstruction efficiency as a function of the local coordinate in the chamber is shown in figure 16

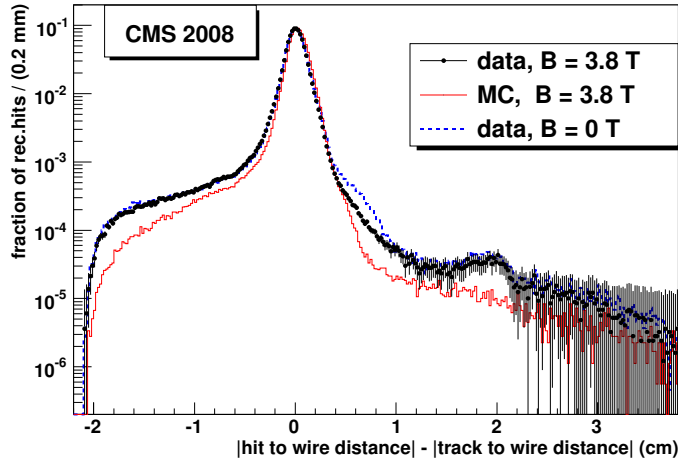


Figure 14. Distribution of the difference between the distance to the cell anode wire of the first hit recorded in a cell and the distance of the extrapolated track position.

for the r - ϕ layers of chambers MB1-MB4 of sector 4 in YB0. The observed decrease of efficiency near the chamber’s edges is due to the fact that a track passing near the boundary but outside the chamber volume can be incorrectly predicted to have its extrapolation inside the chamber. Note that the asymmetric behaviour of the efficiency curve on the opposite sides of a chamber is due to the staggered geometry of the chambers in a sector (see figure 1, bottom part) and to the track selection which requires a confirmation of a good track segment, compatible with track extrapolation, in chamber MB n +1 when chamber MB n is under study. Due to this requirement, the chamber region near one edge of the chamber is not illuminated for MB1, MB2 and MB3. The method can be safely applied to all chambers of the three uppermost and lowermost sectors of the wheels YB–1, YB0 and YB1, where there are enough good quality tracker tracks that allow reliable extrapolation.

The DT chamber efficiency can also be evaluated making use exclusively of the information coming from the muon spectrometer, thus extending the efficiency measurement to the chambers of outer barrel wheels YB \pm 2. Muon tracks are reconstructed with the information provided by neighbouring chambers and extrapolated to the middle of the chamber under test. Two different approaches have been considered to reconstruct the tracks and obtain the extrapolated position. A simple, linear fit to the hits recorded in the other chambers in the same sector was performed, taking into account the uncertainty due to multiple scattering in the iron. The resulting track was extrapolated to the chamber under test. This method is only valid for data taken with no magnetic field, as in this case muons essentially follow a straight line trajectory. For runs taken with the nominal magnetic field we rely on the “Standalone Muon” reconstruction software [21]. In this case, the hits present in the chamber under test take part in the track fitting process, thus potentially biasing the determination of the segment reconstruction efficiency. Results obtained while applying this procedure to runs taken with zero field are, however, compatible with those obtained from the linear tracker extrapolation. To ensure a good accuracy in the track extrapolation and to minimize a potential bias, the following selection criteria were applied:

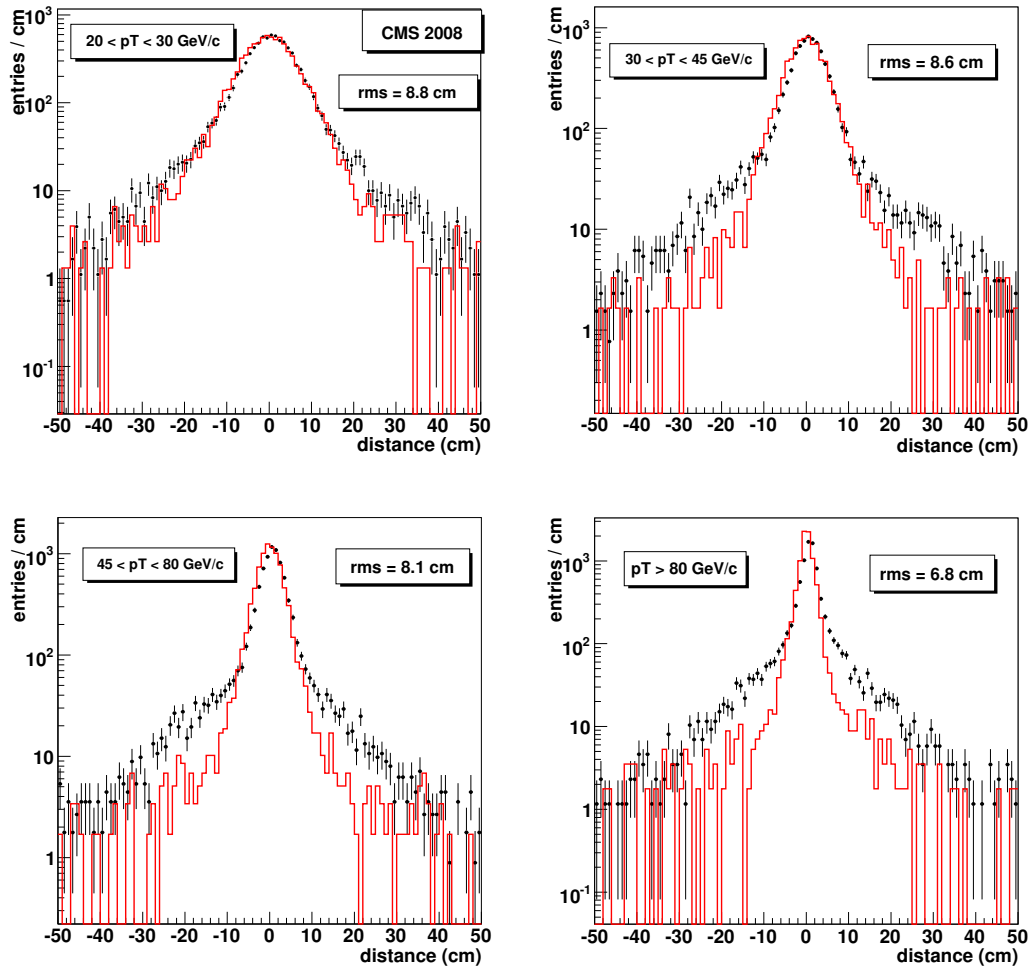


Figure 15. Distance between the extrapolated position from the tracker track and the reconstructed 2D r - ϕ segment position in MB1, for different p_T bins. Dots: real data; full line histograms: simulated data.

- in both r - z and r - ϕ planes the number of hits associated with the muon track was required to be over 4 and 13 hits, respectively, not counting the chamber under study;
- the error on the position of the extrapolation point in the chamber was required to be smaller than 1.5 cm;
- the tracks must cross only a single sector and wheel;
- track segments in the top (bottom) chambers of CMS are selected if the event was triggered on the opposite side, bottom (top) part of the detector, in order to decouple the efficiency study from any potential trigger effects.

Most tracks with high extrapolation error have a low momentum ($p_T < 10 \text{ GeV}/c$), as they are most affected by multiple scattering effects. Given the large amount of data recorded during CRAFT, the number of events left after the selection is sufficient for a good efficiency measurement.

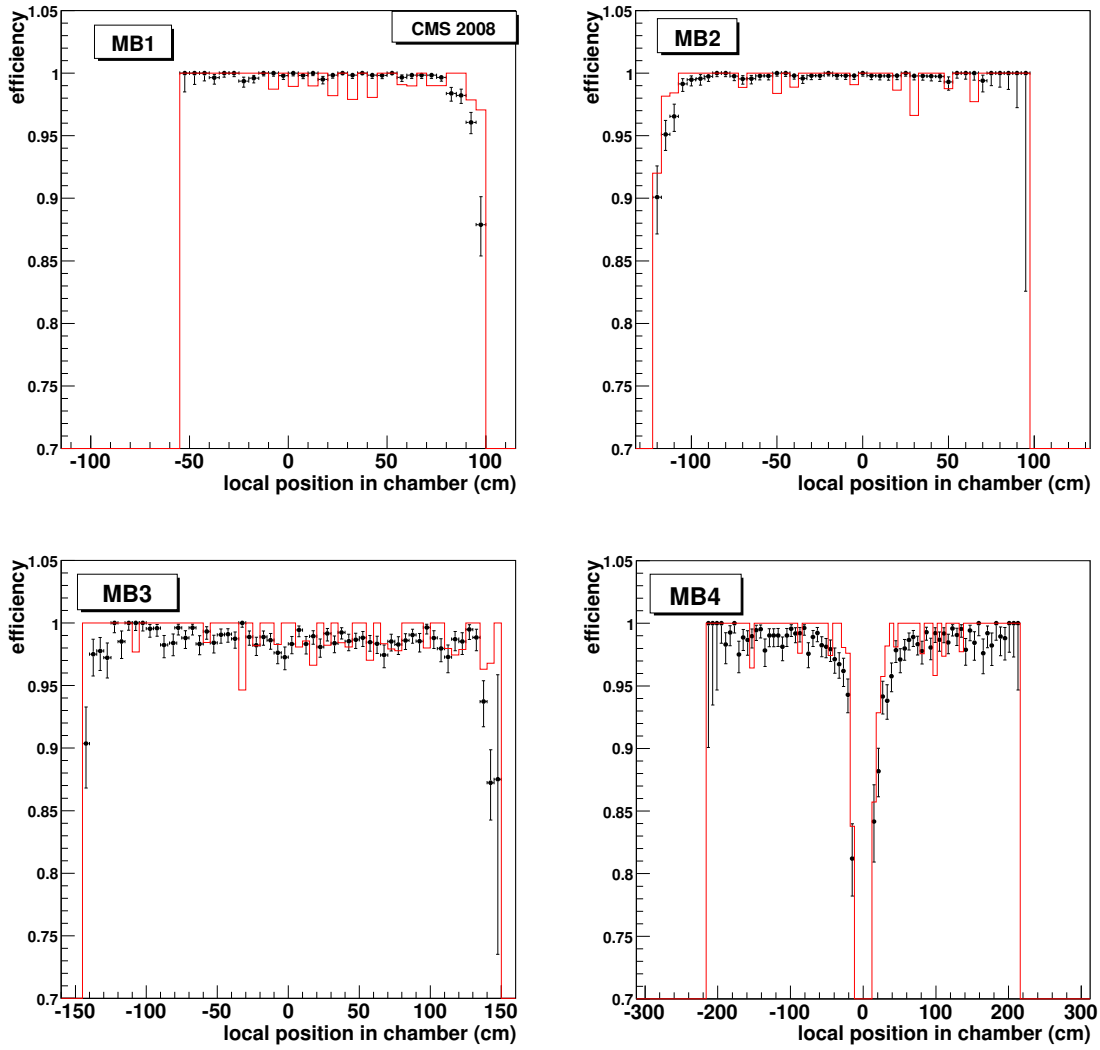


Figure 16. 2D r - ϕ segment efficiency as a function of the local coordinate in the chamber in YB0, sector 4. Dots: real data; full line histograms: simulated data. Note that the MB4 station in this sector is split into two chambers.

A chamber was considered to be efficient when a r - ϕ or r - z segment was found in that chamber within a 5 cm window around the extrapolated position (about 10 times the RMS spread of the distribution of the spatial residuals, see next section). The inefficiency is concentrated at chamber borders, due to geometrical effects. Efficiencies are higher than 99% for the r - ϕ plane once the predicted position from the extrapolation is required to be inside the chamber, at a distance larger than 10 cm from the border (cf. figure 16), in fair agreement with the results obtained using tracker tracks information for all the wheels in which the comparison between the two methods was possible. Efficiencies in the r - z plane are approximately 2% lower, given the smaller number of hits available for segment reconstruction in this plane.

All DT sectors but the vertical ones (sectors 1 and 7) of the five wheels were studied. Figure 17

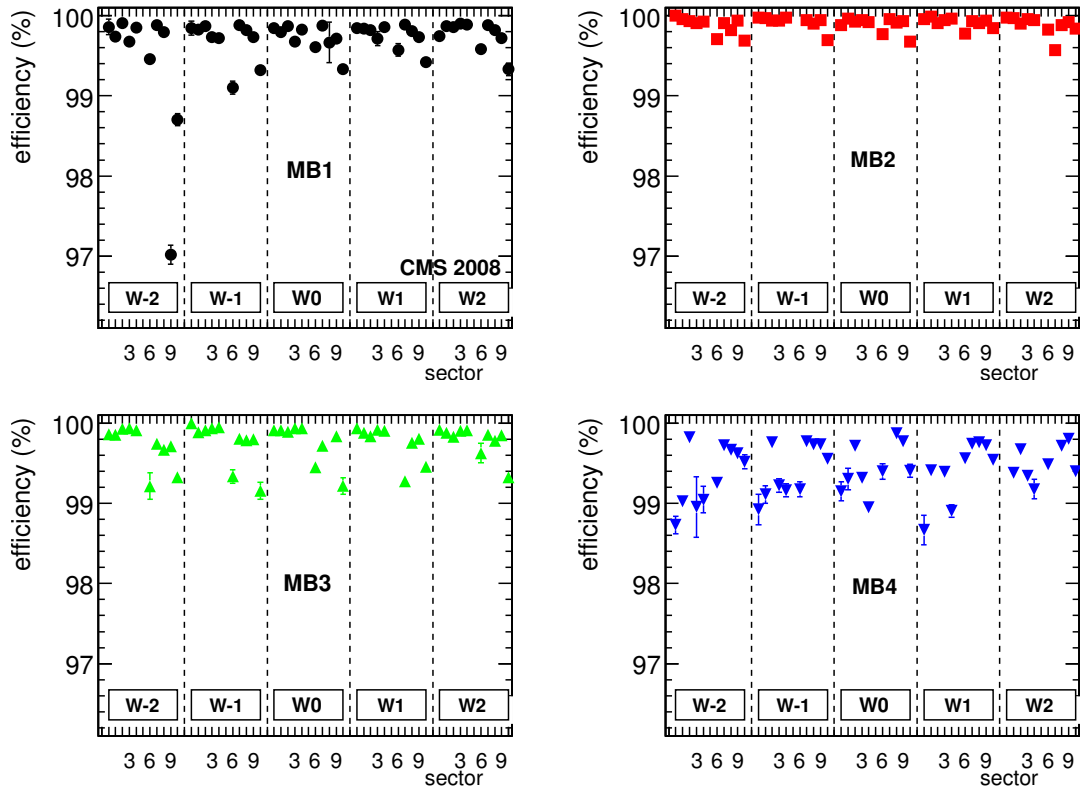


Figure 17. Segment reconstruction efficiency in the r - ϕ planes in the barrel muon chambers, as a function of the sector number for the different wheels.

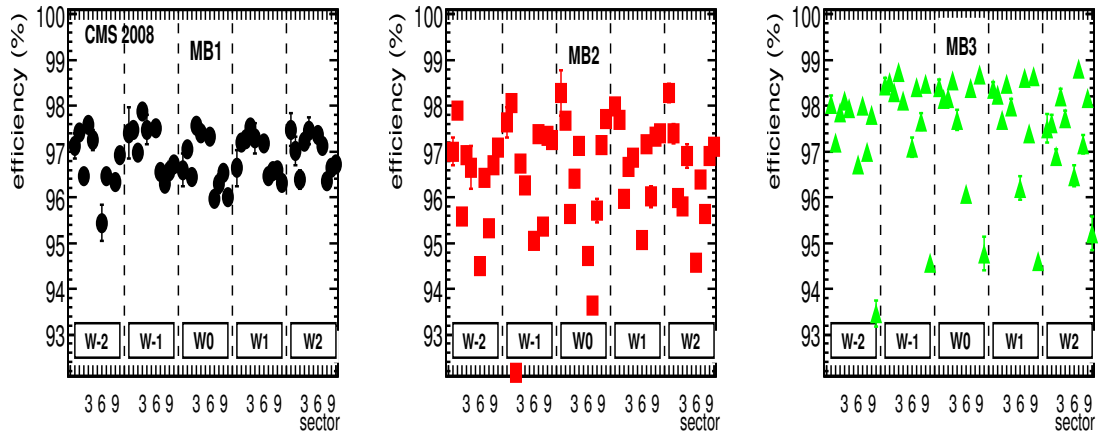


Figure 18. Segment reconstruction efficiency in the r - z planes in the barrel muon chambers, as a function of the sector number for the different wheels.

shows the chamber efficiency in the r - ϕ plane, obtained by the second method described above. Every plot gives the efficiencies for a given station for each sector and wheel analyzed, marked on the horizontal axis. Figure 18 shows the corresponding efficiencies in the r - z plane, for the three chamber types (MB1/2/3) that measure the coordinate of the hit position in this plane. Results on

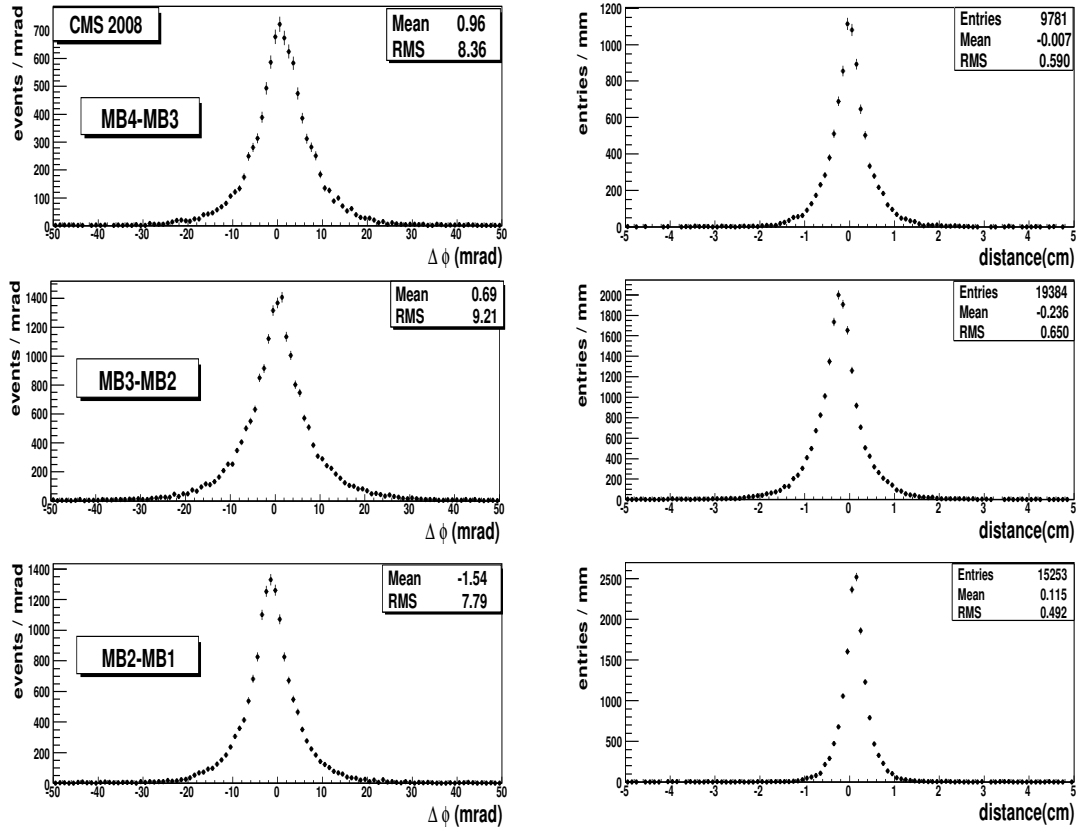


Figure 19. Left: distribution of the difference of the angles in the CMS bending plane of muon track segments reconstructed in consecutive stations in YB-1, sector 4, measured at $B = 0$ T. Right: distribution of the distance between the intersection with the central plane of station MBn of the segment reconstructed in this station and of the extrapolation of the segment reconstructed in station MBn-1.

efficiencies are fully compatible among sectors; the drop of efficiency observed in some of them corresponds to those sectors where the muon incident angle is largest. Results obtained at $B = 0$ T are in agreement with those shown in figures 17 and 18.

6.2 Track segment position and direction measurements

In order to study the quality of the segment reconstruction, the comparison of position and direction measurements between different muon chambers for the same cosmic muon have been performed. First, the data collected with $B = 0$ T were studied. The distributions of the difference of the directions of muon track segments reconstructed in the CMS bending plane in consecutive chambers are shown in figure 19 (left) for the chambers of sector 4 of YB-1. The average values of the distributions are of the order of 1 mrad, due to misalignment effects (both in the internal components of the chambers and on the relative orientation between chambers) which are not yet completely taken into account in the reconstruction. Figure 19 (right) shows the distribution of the distance between the intersection with the central plane of station MBn of the segment reconstructed in this station and of the extrapolation of the segment reconstructed in MBn-1. The average values indicate relative position misalignments between consecutive chambers of the order of a few mil-

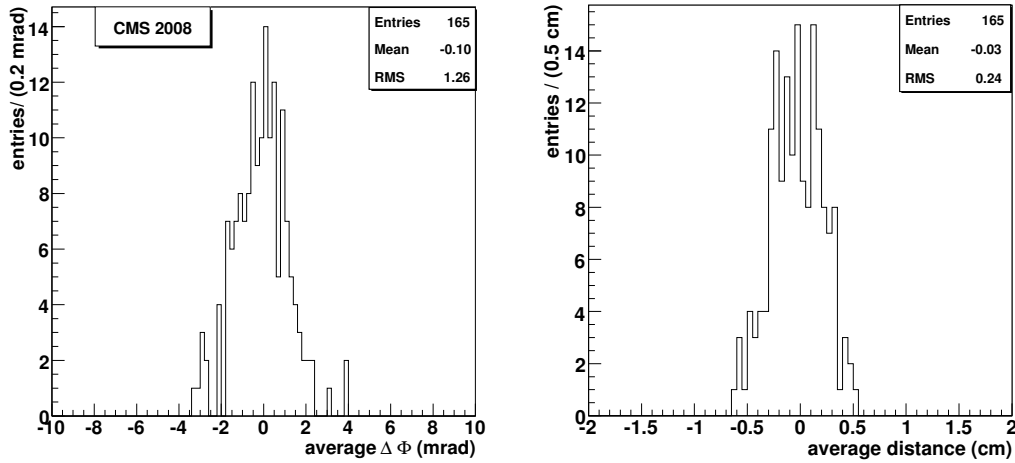


Figure 20. Left: distribution of the averages of the angle differences at $B = 0$ T between consecutive stations in all wheels and sectors. Right: distribution of the averages of the distances at $B = 0$ T between measured and extrapolated positions in consecutive chambers.

limeters. It is worth noting that the smaller dispersion of the position difference for MB1-MB2 chambers (right-bottom plot in the figure) is due to the smaller size of the steel yoke between these chambers, compared to the steel yokes between MB2-MB3 and MB3-MB4.

The summary of the above results for all the wheels and sectors is shown in figure 20. The distribution of the average values of the angle differences is shown in the histogram on the left. The RMS of the distribution is about 1 mrad. The histogram on the right shows a similar plot for the differences between measured and extrapolated positions. The RMS of the distribution is about 2 mm, showing that the relative alignment between the chambers is compatible with the tolerance expected for the mechanical installation of the chambers in CMS. This result guarantees that for the beginning of LHC running the muon L1 trigger processor will operate correctly, efficiently providing muon trigger candidates with reliable estimation of their transverse momentum. Since there is no evidence for chambers placed outside the design mechanical tolerance, we expect that from these start-up mis-alignment conditions the use of survey data and of the data from the laser alignment system [14] will bring the position uncertainty to the design goal of about $100\ \mu\text{m}$ for High Level Trigger and off-line reconstruction. In addition, software alignment procedures using prompt muon tracks have been deployed, which show that it will be possible to reach a comparable accuracy on the chambers' position after accumulating data corresponding to a few pb^{-1} of integrated luminosity [13].

6.3 Bending power measurements

Data with the magnetic field value $B = 3.8$ T in the central solenoid were used to study the bending power of the muon spectrometer. The difference in the track angle measurements between consecutive stations were studied for different values of the transverse momentum of the associated track, which was measured independently by the tracker. These distributions are shown in figure 21 for MB2-MB3 pairs of stations. As seen from the figure, the bending power for a $p_T = 30\ \text{GeV}/c$

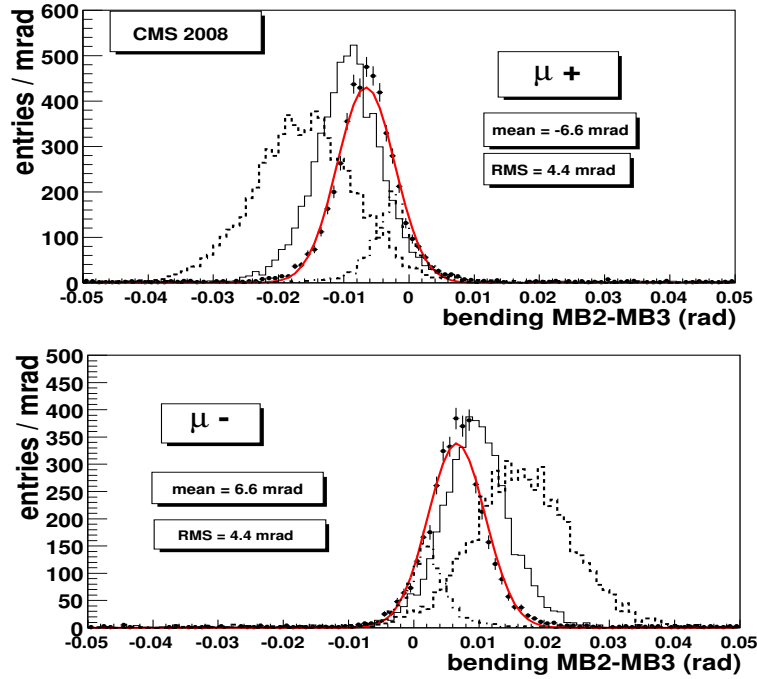


Figure 21. Bending angle differences between MB2 and MB3 stations. Top: μ^+ ; bottom: μ^- . Distributions for different p_T intervals are shown: [8–12] (dashed line), [18–22] (full line), [27–33] (points) and [90–110] GeV/c (dashed-dotted line). The curves show the result of a Gaussian fit to data distribution for the $27 < p_T < 33$ GeV/c sample.

muon is about 6.6 mrad. Similar distributions are observed for MB1-MB2 and MB3-MB4 pairs of stations, with bending power equal to 4.0 mrad and 6.0 mrad, respectively. Note that the width of the magnetized steel between the chambers is about 30 cm between MB1 and MB2 and 62 cm between MB2-MB3 and MB3-MB4 [22]. The magnetic flux density in the steel yokes decreases slightly with the radial position.

Figure 22 shows the distributions of the angle difference between MB1 and MB4 stations, displaying the bending power of the full lever arm in a barrel sector. For muons selected in the p_T range [150, 250] GeV/c, the average deflection by the magnetic field in the steel return yokes of the magnet is about 3.4 mrad.

The above results and a comparison with the simulation are summarized in figures 23 and 24, where the average and the width of the Gaussian fits to the distributions of the angle difference are plotted versus the transverse momentum of the track. The results are shown both for positive (full points) and negative muons (open points). The behaviour shown in figure 24 is consistent with the expectations from the multiple scattering in the iron: the dashed and full lines show respectively the computation for an average material crossed by the muon between the two innermost stations of MB1 and MB2 (18 radiation lengths) and of MB2 and MB3 or MB3 and MB4 (37 radiation lengths) [7], summed in quadrature with a constant term $\sigma_\infty = 2.5$ mrad. This asymptotical value reached at high momenta is compatible with expectations. In fact, the intrinsic angular resolution of each chamber expected from the observed single hit resolution (on average about 290 μm , see figure 9, for the core of the hit residual distribution) is $\sigma_{\text{intrins.}} = 1.5$ mrad, taking into account the

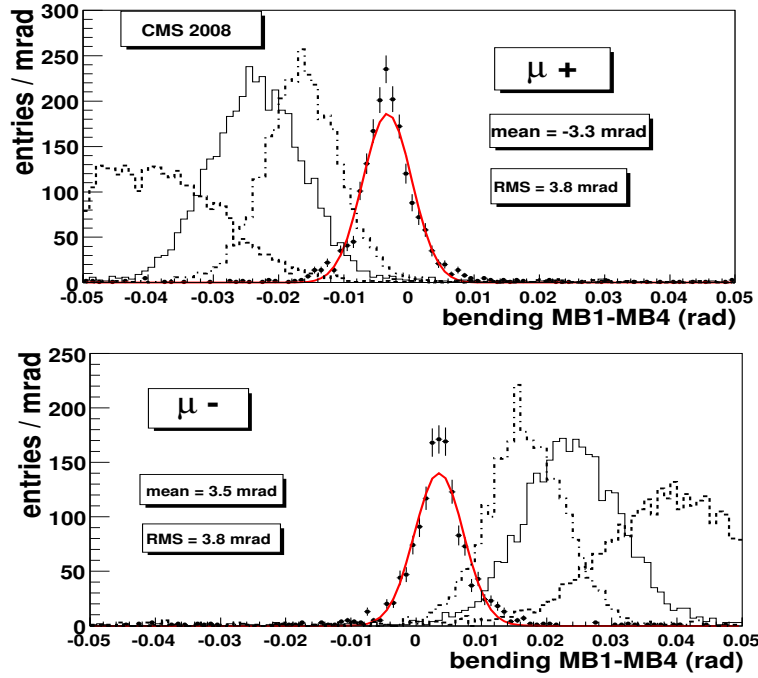


Figure 22. Bending angle differences between MB1 and MB4 stations. Top: μ^+ ; bottom: μ^- . Distributions for different p_T intervals are shown: [8–12] (dashed line), [18–22] (full line), [27–33] (dashed-dotted line) and [150–250] GeV/c (points). The curves show the result of a Gaussian fit to data distribution for the $150 < p_T < 250$ GeV/c sample.

hit multiplicity distributions of the segments and the presence of tails in the hit residual distributions shown in figure 7. The contribution to the bending measurement error from the incomplete knowledge of chambers’ alignment, as extracted from $B = 0$ T data (cf. the distribution of the $\Delta\phi$ averages shown in figure 20) is $\sigma_{mis-align} = 1.3 \text{ mrad}/\sqrt{2} = 0.9 \text{ mrad}$. The expected value for σ_∞ is thus $\sigma_\infty = [\sigma_{intrinsic}^2 + \sigma_{mis-align}^2]^{1/2} \cdot \sqrt{2} = 2.5 \text{ mrad}$. It must be noted that the asymptotic behaviour for MB2-MB3 and MB3-MB4 is slightly worse, mainly due to the fact that the modelling of the multiple scattering effects with a Gaussian curve tends to be inadequate when increasing the amount of material crossed by the muon. The intrinsic angular resolution measured in dedicated bunched test beams [23] was about 1 mrad for muon tracks normal to the chamber plane. It is worth stressing here that the present result is obtained using segment tracks with a very large angular spread with respect to the direction normal to the chambers’ plane, for which the chamber behaviour is optimal. The angular spread of segments originating from prompt muons produced in pp collisions is considerably smaller.

7 Conclusions

The performance of the DT barrel muon detector of CMS was studied in detail using cosmic muon data collected in autumn 2008, both with zero magnetic field and with the magnet solenoid operating at $B = 3.8$ T. The data analysis performed on 246 out of the total of 250 DT chambers shows a very good muon reconstruction capability, with a resolution of single reconstructed hits

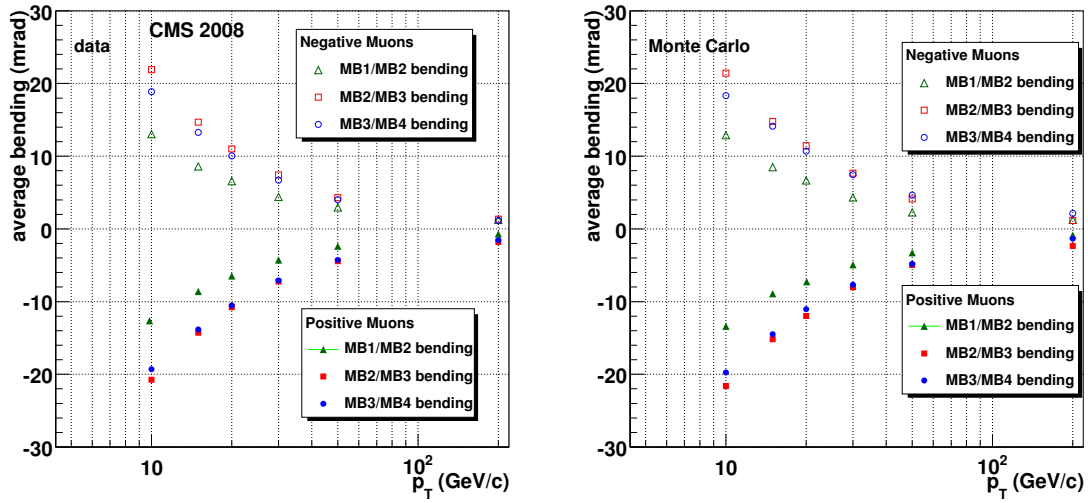


Figure 23. Mean values of Gaussian fits to the distributions of the bending angle differences between consecutive stations as a function of the muon p_T . Data are for the magnetic field value $B = 3.8$ T in the central solenoid. Left: real data; right: simulated data.

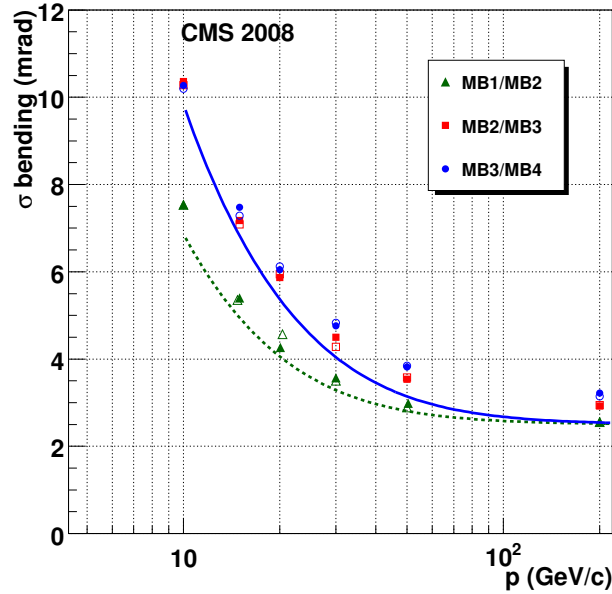


Figure 24. Widths of Gaussian fits to the distributions of the bending angle differences between consecutive stations as a function of the muon momentum. Full points: μ^+ ; open points: μ^- . The dashed (full line) curves show the expectation from multiple scattering between MB1-MB2(MB2-MB3 and MB3-MB4) stations, with 2.5 mrad added in quadrature, corresponding to the asymptotic value extracted at high momenta.

on the order of $260 \mu\text{m}$ in all chambers except the vertical ones, which could not be studied well with cosmic rays. The reconstruction efficiency of high-quality local track segments in each station

has been measured to be about 99% in all chambers. The comparison between measurements of the track segment positions and directions in the different chambers shows a behaviour compatible with the expectations from the multiple scattering of the muons in the steel yoke. The spread in the measurement of the track direction in the bending plane of CMS was about 6 mrad, averaged over the whole momentum spectrum of cosmic muons with $p_T > 10$ GeV/c. The bending power in the steel return yoke between the innermost and outermost station has been measured to be about 3 mrad for $p_T = 200$ GeV/c muons. The relative misalignments of the chambers, as measured by the data collected at $B = 0$ T, are well within the mechanical tolerances (a few mm) for the insertion of the chambers into their cradles inside the magnet yoke structure.

The chamber performance is in good agreement with the simulation; it provides a good starting point that assures fully efficient operation of the muon DT trigger and eventual achievement of the original design criteria of the DT system. The criteria specify robust and efficient muon identification, and the capability of measuring the muon position in each station with a precision of about $100\ \mu\text{m}$, in order to provide good momentum resolution for highly energetic muons. The above results are very encouraging and allow the anticipation of a good performance of the DT barrel muon detector during early phases of LHC operation and data taking, which would provide efficient identification and reconstruction of muons.

Acknowledgments

We thank the technical and administrative staff at CERN and other CMS Institutes, and acknowledge support from: FMSR (Austria); FNRS and FWO (Belgium); CNPq, CAPES, FAPERJ, and FAPESP (Brazil); MES (Bulgaria); CERN; CAS, MoST, and NSFC (China); COLCIENCIAS (Colombia); MSES (Croatia); RPF (Cyprus); Academy of Sciences and NICPB (Estonia); Academy of Finland, ME, and HIP (Finland); CEA and CNRS/IN2P3 (France); BMBF, DFG, and HGF (Germany); GSRT (Greece); OTKA and NKTH (Hungary); DAE and DST (India); IPM (Iran); SFI (Ireland); INFN (Italy); NRF (Korea); LAS (Lithuania); CINVESTAV, CONACYT, SEP, and UASLP-FAI (Mexico); PAEC (Pakistan); SCSR (Poland); FCT (Portugal); JINR (Armenia, Belarus, Georgia, Ukraine, Uzbekistan); MST and MAE (Russia); MSTDS (Serbia); MICINN and CPAN (Spain); Swiss Funding Agencies (Switzerland); NSC (Taipei); TUBITAK and TAEK (Turkey); STFC (United Kingdom); DOE and NSF (USA). Individuals have received support from the Marie-Curie IEF program (European Union); the Leventis Foundation; the A. P. Sloan Foundation; and the Alexander von Humboldt Foundation.

References

- [1] CMS collaboration, *The CMS experiment at the CERN LHC*, 2008 [JINST 3 S08004](#).
- [2] CMS collaboration, *Commissioning of the CMS experiment and the cosmic run at four tesla*, 2010 [JINST 5 T03001](#).
- [3] T. Christiansen, *The CMS magnet test and cosmic challenge*, [CMS-NOTE-2006-076](#) (2006).
- [4] M. Fouz et al., *Measurement of the Drift Velocity in the CMS Barrel Muon Chambers During CMS magnet test and cosmic challenge*, [CMS-NOTE-2008-003](#) (2008).

- [5] M. Aldaya et al., *Measurement of the charge ratio of cosmic muons using CMS data*, [CMS-NOTE-2008-016](#) (2008).
- [6] CMS collaboration, *Performance of CMS muon reconstruction in cosmic-ray events*, [2010 JINST 5 T03022](#).
- [7] CMS collaboration, *The Muon Project Technical Design Report*, [CERN-LHCC-97-032](#) (1997).
- [8] M. Aguilar-Benitez et al., *Construction and test of the final CMS Barrel Drift Tube Muon Chamber prototype*, *Nucl. Instrum. Meth. A* **480** (2002) 658.
- [9] P. Arce et al., *Bunched beam test of the CMS drift tubes local muon trigger*, *Nucl. Instrum. Meth. A* **534** (2004) 441.
- [10] CMS collaboration, *Performance of the CMS drift-tube chamber local trigger with cosmic rays*, [2010 JINST 5 T03003](#).
- [11] P. Biallas et al., *Simulation of Cosmic Muons and Comparison with Data from the Cosmic Challenge using Drift Tube Chambers*, [CMS-NOTE-2007-024](#) (2007).
- [12] J. Puerta-Pelayo et al., *Parameterization of the Response of the Muon Barrel Drift Tubes*, [CMS-NOTE-2005-018](#) (2005).
- [13] CMS collaboration, *Alignment of the CMS muon system with cosmic-ray and beam-halo muons*, [2010 JINST 5 T03020](#).
- [14] CMS collaboration, *Aligning the CMS muon chambers with the muon alignment system during an extended cosmic ray run*, [2010 JINST 5 T03019](#).
- [15] G. Abbiendi et al., *Offline calibration procedure of the CMS drift tube detectors*, [2009 JINST 4 P05002](#).
- [16] CMS collaboration, *Calibration of the CMS drift tube chambers and measurement of the drift velocity with cosmic rays*, [2010 JINST 5 T03016](#).
- [17] N. Amapane et al., *Local Muon Reconstruction in the Drift Tube Detectors*, [CMS-NOTE-2009-008](#) (2009).
- [18] C. Albajar et al., *Test beam analysis of the first CMS drift tube muon chamber*, *Nucl. Instrum. Meth. A* **525** (2004) 465.
- [19] F. Cavallo et al., *Test of MB3 Muon Barrel Drift Chambers with cosmic rays*, [CMS-NOTE-2003-017](#) (2003).
- [20] CMS collaboration, *Fine synchronization of the CMS muon drift-tube local trigger using cosmic rays*, [2010 JINST 5 T03004](#).
- [21] CMS collaboration, *The CMS Physics Technical Design Report, Volume I: Detector Performance and Software*, [CERN-LHCC-2006-001](#) (2006).
- [22] CMS collaboration, *The CMS Magnet Technical Design Report*, [CERN-LHCC-97-010](#) (1997).
- [23] N. Amapane et al., *Comparison of DT testbeam results on Local Track Reconstruction with the OSCAR+ORCA simulation*, [CMS-NOTE-2006-009](#) (2006).

The CMS collaboration

Yerevan Physics Institute, Yerevan, Armenia

S. Chatrchyan, V. Khachatryan, A.M. Sirunyan

Institut für Hochenergiephysik der OeAW, Wien, Austria

W. Adam, B. Arnold, H. Bergauer, T. Bergauer, M. Dragicevic, M. Eichberger, J. Erö, M. Friedl, R. Frühwirth, V.M. Ghete, J. Hammer¹, S. Hänsel, M. Hoch, N. Hörmann, J. Hrubec, M. Jeitler, G. Kasieczka, K. Kastner, M. Krammer, D. Liko, I. Magrans de Abril, I. Mikulec, F. Mittermayr, B. Neuherz, M. Oberegger, M. Padrta, M. Pernicka, H. Rohringer, S. Schmid, R. Schöffbeck, T. Schreiner, R. Stark, H. Steininger, J. Strauss, A. Taurok, F. Teischinger, T. Themel, D. Uhl, P. Wagner, W. Waltenberger, G. Walzel, E. Widl, C.-E. Wulz

National Centre for Particle and High Energy Physics, Minsk, Belarus

V. Chekhovsky, O. Dvornikov, I. Emelianchik, A. Litomin, V. Makarenko, I. Marfin, V. Mossolov, N. Shumeiko, A. Solin, R. Stefanovitch, J. Suarez Gonzalez, A. Tikhonov

Research Institute for Nuclear Problems, Minsk, Belarus

A. Fedorov, A. Karneyeu, M. Korzhik, V. Panov, R. Zuyeuski

Research Institute of Applied Physical Problems, Minsk, Belarus

P. Kuchinsky

Universiteit Antwerpen, Antwerpen, Belgium

W. Beaumont, L. Benucci, M. Cardaci, E.A. De Wolf, E. Delmeire, D. Druzhdin, M. Hashemi, X. Janssen, T. Maes, L. Mucibello, S. Ochesanu, R. Rougny, M. Selvaggi, H. Van Haevermaet, P. Van Mechelen, N. Van Remortel

Vrije Universiteit Brussel, Brussel, Belgium

V. Adler, S. Beauceron, S. Blyweert, J. D'Hondt, S. De Weirtdt, O. Devroede, J. Heyninck, A. Kalogeropoulos, J. Maes, M. Maes, M.U. Mozer, S. Tavernier, W. Van Doninck¹, P. Van Mulders, I. Vilella

Université Libre de Bruxelles, Bruxelles, Belgium

O. Bouhali, E.C. Chabert, O. Charaf, B. Clerboux, G. De Lentdecker, V. Dero, S. Elgammal, A.P.R. Gay, G.H. Hammad, P.E. Marage, S. Rugovac, C. Vander Velde, P. Vanlaer, J. Wickens

Ghent University, Ghent, Belgium

M. Grunewald, B. Klein, A. Marinov, D. Ryckbosch, F. Thyssen, M. Tytgat, L. Vanelderen, P. Verwilligen

Université Catholique de Louvain, Louvain-la-Neuve, Belgium

S. Basegmez, G. Bruno, J. Caudron, C. Delaere, P. Demin, D. Favart, A. Giammanco, G. Grégoire, V. Lemaitre, O. Militaru, S. Ovyn, K. Piotrkowski¹, L. Quertenmont, N. Schul

Université de Mons, Mons, Belgium

N. Beliy, E. Daubie

Centro Brasileiro de Pesquisas Fisicas, Rio de Janeiro, Brazil

G.A. Alves, M.E. Pol, M.H.G. Souza

Universidade do Estado do Rio de Janeiro, Rio de Janeiro, Brazil

W. Carvalho, D. De Jesus Damiao, C. De Oliveira Martins, S. Fonseca De Souza, L. Mundim, V. Oguri, A. Santoro, S.M. Silva Do Amaral, A. Sznajder

Instituto de Fisica Teorica, Universidade Estadual Paulista, Sao Paulo, Brazil

T.R. Fernandez Perez Tomei, M.A. Ferreira Dias, E. M. Gregores², S.F. Novaes

Institute for Nuclear Research and Nuclear Energy, Sofia, Bulgaria

K. Abadjiev¹, T. Anguelov, J. Damgov, N. Darmenov¹, L. Dimitrov, V. Genchev¹, P. Iaydjiev, S. Piperov, S. Stoykova, G. Sultanov, R. Trayanov, I. Vankov

University of Sofia, Sofia, Bulgaria

A. Dimitrov, M. Dyulendarova, V. Kozhuharov, L. Litov, E. Marinova, M. Mateev, B. Pavlov, P. Petkov, Z. Toteva¹

Institute of High Energy Physics, Beijing, China

G.M. Chen, H.S. Chen, W. Guan, C.H. Jiang, D. Liang, B. Liu, X. Meng, J. Tao, J. Wang, Z. Wang, Z. Xue, Z. Zhang

State Key Lab. of Nucl. Phys. and Tech., Peking University, Beijing, China

Y. Ban, J. Cai, Y. Ge, S. Guo, Z. Hu, Y. Mao, S.J. Qian, H. Teng, B. Zhu

Universidad de Los Andes, Bogota, Colombia

C. Avila, M. Baquero Ruiz, C.A. Carrillo Montoya, A. Gomez, B. Gomez Moreno, A.A. Ocampo Rios, A.F. Osorio Oliveros, D. Reyes Romero, J.C. Sanabria

Technical University of Split, Split, Croatia

N. Godinovic, K. Lelas, R. Plestina, D. Polic, I. Puljak

University of Split, Split, Croatia

Z. Antunovic, M. Dzelalija

Institute Rudjer Boskovic, Zagreb, Croatia

V. Brigljevic, S. Duric, K. Kadija, S. Morovic

University of Cyprus, Nicosia, Cyprus

R. Fereos, M. Galanti, J. Mousa, A. Papadakis, F. Ptochos, P.A. Razis, D. Tsiakkouri, Z. Zinonos

National Institute of Chemical Physics and Biophysics, Tallinn, Estonia

A. Hektor, M. Kadastik, K. Kannike, M. Müntel, M. Raidal, L. Rebane

Helsinki Institute of Physics, Helsinki, Finland

E. Anttila, S. Czellar, J. Härkönen, A. Heikkinen, V. Karimäki, R. Kinnunen, J. Klem, M.J. Kortelainen, T. Lampén, K. Lassila-Perini, S. Lehti, T. Lindén, P. Luukka, T. Mäenpää, J. Nysten, E. Tuominen, J. Tuominiemi, D. Ungaro, L. Wendland

Lappeenranta University of Technology, Lappeenranta, Finland

K. Banzuzi, A. Korpela, T. Tuuva

Laboratoire d'Annecy-le-Vieux de Physique des Particules, IN2P3-CNRS, Annecy-le-Vieux, France

P. Nedelec, D. Sillou

DSM/IRFU, CEA/Saclay, Gif-sur-Yvette, France

M. Besancon, R. Chipaux, M. Dejardin, D. Denegri, J. Descamps, B. Fabbro, J.L. Faure, F. Ferri, S. Ganjour, F.X. Gentit, A. Givernaud, P. Gras, G. Hamel de Monchenault, P. Jarry, M.C. Lemaire, E. Locci, J. Malcles, M. Marionneau, L. Millischer, J. Rander, A. Rosowsky, D. Rousseau, M. Titov, P. Verrecchia

Laboratoire Leprince-Ringuet, Ecole Polytechnique, IN2P3-CNRS, Palaiseau, France

S. Baffioni, L. Bianchini, M. Bluj³, P. Busson, C. Charlot, L. Dobrzynski, R. Granier de Cassagnac, M. Haguenaue, P. Miné, P. Paganini, Y. Sirois, C. Thiebaux, A. Zabi

Institut Pluridisciplinaire Hubert Curien, Université de Strasbourg, Université de Haute Alsace Mulhouse, CNRS/IN2P3, Strasbourg, France

J.-L. Agram⁴, A. Besson, D. Bloch, D. Bodin, J.-M. Brom, E. Conte⁴, F. Drouhin⁴, J.-C. Fontaine⁴, D. Gelé, U. Goerlach, L. Gross, P. Juillot, A.-C. Le Bihan, Y. Patois, J. Speck, P. Van Hove

Université de Lyon, Université Claude Bernard Lyon 1, CNRS-IN2P3, Institut de Physique Nucléaire de Lyon, Villeurbanne, France

C. Baty, M. Bedjidian, J. Blaha, G. Boudoul, H. Brun, N. Chanon, R. Chierici, D. Contardo, P. Depasse, T. Dupasquier, H. El Mamouni, F. Fassi⁵, J. Fay, S. Gascon, B. Ille, T. Kurca, T. Le Grand, M. Lethuillier, N. Lumb, L. Mirabito, S. Perries, M. Vander Donckt, P. Verdier

E. Andronikashvili Institute of Physics, Academy of Science, Tbilisi, Georgia

N. Djaoshvili, N. Roinishvili, V. Roinishvili

Institute of High Energy Physics and Informatization, Tbilisi State University, Tbilisi, Georgia

N. Amaglobeli

RWTH Aachen University, I. Physikalisches Institut, Aachen, Germany

R. Adolphi, G. Anagnostou, R. Brauer, W. Braunschweig, M. Edelhoff, H. Esser, L. Feld, W. Karpinski, A. Khomich, K. Klein, N. Mohr, A. Ostapchouk, D. Pandoulas, G. Pierschel, F. Raupach, S. Schael, A. Schultz von Dratzig, G. Schwering, D. Sprenger, M. Thomas, M. Weber, B. Wittmer, M. Wlochal

RWTH Aachen University, III. Physikalisches Institut A, Aachen, Germany

O. Actis, G. Altenhöfer, W. Bender, P. Biallass, M. Erdmann, G. Fetchenhauer¹, J. Frangenheim, T. Hebbeker, G. Hilgers, A. Hinzmann, K. Hoepfner, C. Hof, M. Kirsch, T. Klimkovich, P. Kreuzer¹, D. Lanske[†], M. Merschmeyer, A. Meyer, B. Philipps, H. Pieta, H. Reithler, S.A. Schmitz, L. Sonnenschein, M. Sowa, J. Steggemann, H. Szczesny, D. Teyssier, C. Zeidler

RWTH Aachen University, III. Physikalisches Institut B, Aachen, Germany

M. Bontenackels, M. Davids, M. Duda, G. Flügge, H. Geenen, M. Giffels, W. Haj Ahmad, T. Hermanns, D. Heydhausen, S. Kalinin, T. Kress, A. Linn, A. Nowack, L. Perchalla, M. Poettgens, O. Pooth, P. Sauerland, A. Stahl, D. Tornier, M.H. Zoeller

Deutsches Elektronen-Synchrotron, Hamburg, Germany

M. Aldaya Martin, U. Behrens, K. Borras, A. Campbell, E. Castro, D. Dammann, G. Eckerlin, A. Flossdorf, G. Flucke, A. Geiser, D. Hatton, J. Hauk, H. Jung, M. Kasemann, I. Katkov, C. Kleinwort, H. Kluge, A. Knutsson, E. Kuznetsova, W. Lange, W. Lohmann, R. Mankel¹,

M. Marienfeld, A.B. Meyer, S. Miglioranza, J. Mnich, M. Ohlerich, J. Olzem, A. Parenti, C. Rosemann, R. Schmidt, T. Schoerner-Sadenius, D. Volyanskyy, C. Wissing, W.D. Zeuner¹

University of Hamburg, Hamburg, Germany

C. Autermann, F. Bechtel, J. Draeger, D. Eckstein, U. Gebbert, K. Kaschube, G. Kaussen, R. Klanner, B. Mura, S. Naumann-Emme, F. Nowak, U. Pein, C. Sander, P. Schleper, T. Schum, H. Stadie, G. Steinbrück, J. Thomsen, R. Wolf

Institut für Experimentelle Kernphysik, Karlsruhe, Germany

J. Bauer, P. Blüm, V. Buege, A. Cakir, T. Chwalek, W. De Boer, A. Dierlamm, G. Dirkes, M. Feindt, U. Felzmann, M. Frey, A. Furgeri, J. Gruschke, C. Hackstein, F. Hartmann¹, S. Heier, M. Heinrich, H. Held, D. Hirschbuehl, K.H. Hoffmann, S. Honc, C. Jung, T. Kuhr, T. Liamsuwan, D. Martschei, S. Mueller, Th. Müller, M.B. Neuland, M. Niegel, O. Oberst, A. Oehler, J. Ott, T. Peiffer, D. Piparo, G. Quast, K. Rabbertz, F. Ratnikov, N. Ratnikova, M. Renz, C. Saout¹, G. Sartisohn, A. Scheurer, P. Schieferdecker, F.-P. Schilling, G. Schott, H.J. Simonis, F.M. Stober, P. Sturm, D. Troendle, A. Trunov, W. Wagner, J. Wagner-Kuhr, M. Zeise, V. Zhukov⁶, E.B. Ziebarth

Institute of Nuclear Physics "Demokritos", Aghia Paraskevi, Greece

G. Daskalakis, T. Geralis, K. Karafasoulis, A. Kyriakis, D. Loukas, A. Markou, C. Markou, C. Mavrommatis, E. Petrakou, A. Zachariadou

University of Athens, Athens, Greece

L. Gouskos, P. Katsas, A. Panagiotou¹

University of Ioánnina, Ioánnina, Greece

I. Evangelou, P. Kokkas, N. Manthos, I. Papadopoulos, V. Patras, F.A. Triantis

KFKI Research Institute for Particle and Nuclear Physics, Budapest, Hungary

G. Bencze¹, L. Boldizsar, G. Debreczeni, C. Hajdu¹, S. Hernath, P. Hidas, D. Horvath⁷, K. Krajczar, A. Laszlo, G. Patay, F. Sikler, N. Toth, G. Vesztergombi

Institute of Nuclear Research ATOMKI, Debrecen, Hungary

N. Beni, G. Christian, J. Imrek, J. Molnar, D. Novak, J. Palinkas, G. Szekely, Z. Szillasi¹, K. Tokesi, V. Veszpremi

University of Debrecen, Debrecen, Hungary

A. Kapusi, G. Marian, P. Raics, Z. Szabo, Z.L. Trocsanyi, B. Ujvari, G. Zilizi

Panjab University, Chandigarh, India

S. Bansal, H.S. Bawa, S.B. Beri, V. Bhatnagar, M. Jindal, M. Kaur, R. Kaur, J.M. Kohli, M.Z. Mehta, N. Nishu, L.K. Saini, A. Sharma, A. Singh, J.B. Singh, S.P. Singh

University of Delhi, Delhi, India

S. Ahuja, S. Arora, S. Bhattacharya⁸, S. Chauhan, B.C. Choudhary, P. Gupta, S. Jain, S. Jain, M. Jha, A. Kumar, K. Ranjan, R.K. Shivpuri, A.K. Srivastava

Bhabha Atomic Research Centre, Mumbai, India

R.K. Choudhury, D. Dutta, S. Kailas, S.K. Kataria, A.K. Mohanty, L.M. Pant, P. Shukla, A. Topkar

Tata Institute of Fundamental Research - EHEP, Mumbai, India

T. Aziz, M. Guchait⁹, A. Gurtu, M. Maity¹⁰, D. Majumder, G. Majumder, K. Mazumdar, A. Nayak, A. Saha, K. Sudhakar

Tata Institute of Fundamental Research - HECR, Mumbai, India

S. Banerjee, S. Dugad, N.K. Mondal

Institute for Studies in Theoretical Physics & Mathematics (IPM), Tehran, Iran

H. Arfaei, H. Bakhshiansohi, A. Fahim, A. Jafari, M. Mohammadi Najafabadi, A. Moshaii, S. Paktinat Mehdiabadi, S. Rouhani, B. Safarzadeh, M. Zeinali

University College Dublin, Dublin, Ireland

M. Felcini

INFN Sezione di Bari ^a, Università di Bari ^b, Politecnico di Bari ^c, Bari, Italy

M. Abbrescia^{a,b}, L. Barbone^a, F. Chiumarulo^a, A. Clemente^a, A. Colaleo^a, D. Creanza^{a,c}, G. Cuscela^a, N. De Filippis^a, M. De Palma^{a,b}, G. De Robertis^a, G. Donvito^a, F. Fedele^a, L. Fiore^a, M. Franco^a, G. Iaselli^{a,c}, N. Lacalamita^a, F. Loddo^a, L. Lusito^{a,b}, G. Maggi^{a,c}, M. Maggi^a, N. Manna^{a,b}, B. Marangelli^{a,b}, S. My^{a,c}, S. Natali^{a,b}, S. Nuzzo^{a,b}, G. Papagni^a, S. Piccolomo^a, G.A. Pierro^a, C. Pinto^a, A. Pompili^{a,b}, G. Pugliese^{a,c}, R. Rajan^a, A. Ranieri^a, F. Romano^{a,c}, G. Roselli^{a,b}, G. Selvaggi^{a,b}, Y. Shinde^a, L. Silvestris^a, S. Tupputi^{a,b}, G. Zito^a

INFN Sezione di Bologna ^a, Università di Bologna ^b, Bologna, Italy

G. Abbiendi^a, W. Bacchi^{a,b}, A.C. Benvenuti^a, M. Boldini^a, D. Bonacorsi^a, S. Braibant-Giacomelli^{a,b}, V.D. Cafaro^a, S.S. Caiazza^a, P. Capiluppi^{a,b}, A. Castro^{a,b}, F.R. Cavallo^a, G. Codispoti^{a,b}, M. Cuffiani^{a,b}, I. D'Antone^a, G.M. Dallavalle^{a,1}, F. Fabbri^a, A. Fanfani^{a,b}, D. Fasanella^a, P. Giacomelli^a, V. Giordano^a, M. Giunta^{a,1}, C. Grandi^a, M. Guerzoni^a, S. Marcellini^a, G. Masetti^{a,b}, A. Montanari^a, F.L. Navarria^{a,b}, F. Odorici^a, G. Pellegrini^a, A. Perrotta^a, A.M. Rossi^{a,b}, T. Rovelli^{a,b}, G. Siroli^{a,b}, G. Torromeo^a, R. Travaglini^{a,b}

INFN Sezione di Catania ^a, Università di Catania ^b, Catania, Italy

S. Albergo^{a,b}, S. Costa^{a,b}, R. Potenza^{a,b}, A. Tricomi^{a,b}, C. Tuve^a

INFN Sezione di Firenze ^a, Università di Firenze ^b, Firenze, Italy

G. Barbagli^a, G. Broccolo^{a,b}, V. Ciulli^{a,b}, C. Civinini^a, R. D'Alessandro^{a,b}, E. Focardi^{a,b}, S. Frosali^{a,b}, E. Gallo^a, C. Genta^{a,b}, G. Landi^{a,b}, P. Lenzi^{a,b,1}, M. Meschini^a, S. Paoletti^a, G. Sguazzoni^a, A. Tropiano^a

INFN Laboratori Nazionali di Frascati, Frascati, Italy

L. Benussi, M. Bertani, S. Bianco, S. Colafranceschi¹¹, D. Colonna¹¹, F. Fabbri, M. Giaroni, L. Passamonti, D. Piccolo, D. Pierluigi, B. Ponzio, A. Russo

INFN Sezione di Genova, Genova, Italy

P. Fabbricatore, R. Musenich

INFN Sezione di Milano-Bicocca ^a, Università di Milano-Bicocca ^b, Milano, Italy

A. Benaglia^a, M. Calloni^a, G.B. Cerati^{a,b,1}, P. D'Angelo^a, F. De Guio^a, F.M. Farina^a, A. Ghezzi^a, P. Govoni^{a,b}, M. Malberti^{a,b,1}, S. Malvezzi^a, A. Martelli^a, D. Menasce^a, V. Miccio^{a,b}, L. Moroni^a, P. Negri^{a,b}, M. Paganoni^{a,b}, D. Pedrini^a, A. Pullia^{a,b}, S. Ragazzi^{a,b}, N. Redaelli^a, S. Sala^a, R. Salerno^{a,b}, T. Tabarelli de Fatis^{a,b}, V. Tancini^{a,b}, S. Taroni^{a,b}

INFN Sezione di Napoli ^a, Università di Napoli "Federico II" ^b, Napoli, Italy

S. Buontempo^a, N. Cavallo^a, A. Cimmino^{a,b,1}, M. De Gruttola^{a,b,1}, F. Fabozzi^{a,12}, A.O.M. Iorio^a, L. Lista^a, D. Lomidze^a, P. Noli^{a,b}, P. Paolucci^a, C. Sciacca^{a,b}

INFN Sezione di Padova ^a, Università di Padova ^b, Padova, Italy

P. Azzi^{a,1}, N. Bacchetta^a, L. Barcellan^a, P. Bellan^{a,b,1}, M. Bellato^a, M. Benettoni^a, M. Biasotto^{a,13}, D. Bisello^{a,b}, E. Borsato^{a,b}, A. Branca^a, R. Carlin^{a,b}, L. Castellani^a, P. Checchia^a, E. Conti^a, F. Dal Corso^a, M. De Mattia^{a,b}, T. Dorigo^a, U. Dosselli^a, F. Fanzago^a, F. Gasparini^{a,b}, U. Gasparini^{a,b}, P. Giubilato^{a,b}, F. Gonella^a, A. Gresele^{a,14}, M. Gulmini^{a,13}, A. Kaminskiy^{a,b}, S. Lacaprara^{a,13}, I. Lazzizzera^{a,14}, M. Margoni^{a,b}, G. Maron^{a,13}, S. Mattiazzo^{a,b}, M. Mazzucato^a, M. Meneghelli^a, A.T. Meneguzzo^{a,b}, M. Michelotto^a, F. Montecassiano^a, M. Nespolo^a, M. Passaseo^a, M. Pegoraro^a, L. Perrozzi^a, N. Pozzobon^{a,b}, P. Ronchese^{a,b}, F. Simonetto^{a,b}, N. Toniolo^a, E. Torassa^a, M. Tosi^{a,b}, A. Triossi^a, S. Vanini^{a,b}, S. Ventura^a, P. Zotto^{a,b}, G. Zumerle^{a,b}

INFN Sezione di Pavia ^a, Università di Pavia ^b, Pavia, Italy

P. Baesso^{a,b}, U. Berzano^a, S. Bricola^a, M.M. Necchi^{a,b}, D. Pagano^{a,b}, S.P. Ratti^{a,b}, C. Riccardi^{a,b}, P. Torre^{a,b}, A. Vicini^a, P. Vitulo^{a,b}, C. Viviani^{a,b}

INFN Sezione di Perugia ^a, Università di Perugia ^b, Perugia, Italy

D. Aisa^a, S. Aisa^a, E. Babucci^a, M. Biasini^{a,b}, G.M. Bilei^a, B. Caponeri^{a,b}, B. Checcucci^a, N. Dinu^a, L. Fanò^a, L. Farnesini^a, P. Lariccia^{a,b}, A. Lucaroni^{a,b}, G. Mantovani^{a,b}, A. Nappi^{a,b}, A. Piluso^a, V. Postolache^a, A. Santocchia^{a,b}, L. Servoli^a, D. Tonoiu^a, A. Vedae^a, R. Volpe^{a,b}

INFN Sezione di Pisa ^a, Università di Pisa ^b, Scuola Normale Superiore di Pisa ^c, Pisa, Italy

P. Azzurri^{a,c}, G. Bagliesi^a, J. Bernardini^{a,b}, L. Berretta^a, T. Boccali^a, A. Bocci^{a,c}, L. Borrello^{a,c}, F. Bosi^a, F. Calzolari^a, R. Castaldi^a, R. Dell'Orso^a, F. Fiori^{a,b}, L. Foà^{a,c}, S. Gennai^{a,c}, A. Giassi^a, A. Kraan^a, F. Ligabue^{a,c}, T. Lomtadze^a, F. Mariani^a, L. Martini^a, M. Massa^a, A. Messineo^{a,b}, A. Moggi^a, F. Palla^a, F. Palmonari^a, G. Petraghani^a, G. Petrucciani^{a,c}, F. Raffaelli^a, S. Sarkar^a, G. Segneri^a, A.T. Serban^a, P. Spagnolo^{a,1}, R. Turchini^{a,1}, S. Tolaini^a, G. Tonelli^{a,b,1}, A. Venturi^a, P.G. Verdini^a

INFN Sezione di Roma ^a, Università di Roma "La Sapienza" ^b, Roma, Italy

S. Baccaro^{a,15}, L. Barone^{a,b}, A. Bartoloni^a, F. Cavallari^{a,1}, I. Dafinei^a, D. Del Re^{a,b}, E. Di Marco^{a,b}, M. Diemoz^a, D. Franci^{a,b}, E. Longo^{a,b}, G. Organtini^{a,b}, A. Palma^{a,b}, F. Pandolfi^{a,b}, R. Paramatti^{a,1}, F. Pellegrino^a, S. Rahatlou^{a,b}, C. Rovelli^a

INFN Sezione di Torino ^a, Università di Torino ^b, Università del Piemonte Orientale (Novara) ^c, Torino, Italy

G. Alampi^a, N. Amapane^{a,b}, R. Arcidiacono^{a,b}, S. Argiro^{a,b}, M. Arneodo^{a,c}, C. Biino^a, M.A. Borgia^{a,b}, C. Botta^{a,b}, N. Cartiglia^a, R. Castello^{a,b}, G. Cerminara^{a,b}, M. Costa^{a,b}, D. Dattola^a, G. Dellacasa^a, N. Demaria^a, G. Dughera^a, F. Dumitrache^a, A. Graziano^{a,b}, C. Mariotti^a, M. Marone^{a,b}, S. Maselli^a, E. Migliore^{a,b}, G. Mila^{a,b}, V. Monaco^{a,b}, M. Musich^{a,b}, M. Nervo^{a,b}, M.M. Obertino^{a,c}, S. Oggero^{a,b}, R. Panero^a, N. Pastrone^a, M. Pelliccioni^{a,b}, A. Romero^{a,b}, M. Ruspa^{a,c}, R. Sacchi^{a,b}, A. Solano^{a,b}, A. Staiano^a, P.P. Trapani^{a,b,1}, D. Trocino^{a,b}, A. Vilela Pereira^{a,b}, L. Visca^{a,b}, A. Zampieri^a

INFN Sezione di Trieste ^a, Università di Trieste ^b, Trieste, Italy

F. Ambroglini^{a,b}, S. Belforte^a, F. Cossutti^a, G. Della Ricca^{a,b}, B. Gobbo^a, A. Penzo^a

Kyungpook National University, Daegu, Korea

S. Chang, J. Chung, D.H. Kim, G.N. Kim, D.J. Kong, H. Park, D.C. Son

Wonkwang University, Iksan, Korea

S.Y. Bahk

Chonnam National University, Kwangju, Korea

S. Song

Konkuk University, Seoul, Korea

S.Y. Jung

Korea University, Seoul, Korea

B. Hong, H. Kim, J.H. Kim, K.S. Lee, D.H. Moon, S.K. Park, H.B. Rhee, K.S. Sim

Seoul National University, Seoul, Korea

J. Kim

University of Seoul, Seoul, Korea

M. Choi, G. Hahn, I.C. Park

Sungkyunkwan University, Suwon, Korea

S. Choi, Y. Choi, J. Goh, H. Jeong, T.J. Kim, J. Lee, S. Lee

Vilnius University, Vilnius, Lithuania

M. Janulis, D. Martisiute, P. Petrov, T. Sabonis

Centro de Investigacion y de Estudios Avanzados del IPN, Mexico City, MexicoH. Castilla Valdez¹, A. Sánchez Hernández**Universidad Iberoamericana, Mexico City, Mexico**

S. Carrillo Moreno

Universidad Autónoma de San Luis Potosí, San Luis Potosí, Mexico

A. Morelos Pineda

University of Auckland, Auckland, New Zealand

P. Allfrey, R.N.C. Gray, D. Krofcheck

University of Canterbury, Christchurch, New Zealand

N. Bernardino Rodrigues, P.H. Butler, T. Signal, J.C. Williams

National Centre for Physics, Quaid-I-Azam University, Islamabad, Pakistan

M. Ahmad, I. Ahmed, W. Ahmed, M.I. Asghar, M.I.M. Awan, H.R. Hoorani, I. Hussain, W.A. Khan, T. Khurshid, S. Muhammad, S. Qazi, H. Shahzad

Institute of Experimental Physics, Warsaw, PolandM. Cwiok, R. Dabrowski, W. Dominik, K. Doroba, M. Konecki, J. Krolikowski, K. Pozniak¹⁶, R. Romaniuk, W. Zabolotny¹⁶, P. Zych**Soltan Institute for Nuclear Studies, Warsaw, Poland**

T. Frueboes, R. Gokieli, L. Gosciolo, M. Górski, M. Kazana, K. Nawrocki, M. Szleper, G. Wrochna, P. Zalewski

Laboratório de Instrumentação e Física Experimental de Partículas, Lisboa, Portugal

N. Almeida, L. Antunes Pedro, P. Bargassa, A. David, P. Faccioli, P.G. Ferreira Parracho, M. Freitas Ferreira, M. Gallinaro, M. Guerra Jordao, P. Martins, G. Mini, P. Musella, J. Pela, L. Raposo, P.Q. Ribeiro, S. Sampaio, J. Seixas, J. Silva, P. Silva, D. Soares, M. Sousa, J. Varela, H.K. Wöhri

Joint Institute for Nuclear Research, Dubna, Russia

I. Altsybeev, I. Belotelov, P. Bunin, Y. Ershov, I. Filozova, M. Finger, M. Finger Jr., A. Golunov, I. Golutvin, N. Gorbounov, V. Kalagin, A. Kamenev, V. Karjavin, V. Konoplyanikov, V. Korenkov, G. Kozlov, A. Kurenkov, A. Lanev, A. Makankin, V.V. Mitsyn, P. Moisenz, E. Nikonov, D. Oleynik, V. Palichik, V. Perelygin, A. Petrosyan, R. Semenov, S. Shmatov, V. Smirnov, D. Smolin, E. Tikhonenko, S. Vasil'ev, A. Vishnevskiy, A. Volodko, A. Zarubin, V. Zhiltsov

Petersburg Nuclear Physics Institute, Gatchina (St Petersburg), Russia

N. Bondar, L. Chtchipounov, A. Denisov, Y. Gavrikov, G. Gavrillov, V. Golovtsov, Y. Ivanov, V. Kim, V. Kozlov, P. Levchenko, G. Obrant, E. Orishchin, A. Petrunin, Y. Shcheglov, A. Shchetkovskiy, V. Sknar, I. Smirnov, V. Sulimov, V. Tarakanov, L. Uvarov, S. Vavilov, G. Velichko, S. Volkov, A. Vorobyev

Institute for Nuclear Research, Moscow, Russia

Yu. Andreev, A. Anisimov, P. Antipov, A. Dermenev, S. Gninenko, N. Golubev, M. Kirsanov, N. Krasnikov, V. Matveev, A. Pashenkov, V.E. Postoev, A. Solovey, A. Solovey, A. Toropin, S. Troitsky

Institute for Theoretical and Experimental Physics, Moscow, Russia

A. Baud, V. Epshteyn, V. Gavrillov, N. Ilina, V. Kaftanov[†], V. Kolosov, M. Kossov¹, A. Krokhotin, S. Kuleshov, A. Oulianov, G. Safronov, S. Semenov, I. Shreyber, V. Stolin, E. Vlasov, A. Zhokin

Moscow State University, Moscow, Russia

E. Boos, M. Dubinin¹⁷, L. Dudko, A. Ershov, A. Gribushin, V. Klyukhin, O. Kodolova, I. Lokhtin, S. Petrushanko, L. Sarycheva, V. Savrin, A. Snigirev, I. Vardanyan

P.N. Lebedev Physical Institute, Moscow, Russia

I. Dremin, M. Kirakosyan, N. Konovalova, S.V. Rusakov, A. Vinogradov

State Research Center of Russian Federation, Institute for High Energy Physics, Protvino, Russia

S. Akimenko, A. Artamonov, I. Azhgirey, S. Bitioukov, V. Burtovoy, V. Grishin¹, V. Kachanov, D. Konstantinov, V. Krychkine, A. Levine, I. Lobov, V. Lukanin, Y. Mel'nik, V. Petrov, R. Ryutin, S. Slabospitsky, A. Sobol, A. Sytine, L. Tourtchanovitch, S. Troshin, N. Tyurin, A. Uzunian, A. Volkov

Vinca Institute of Nuclear Sciences, Belgrade, Serbia

P. Adzic, M. Djordjevic, D. Jovanovic¹⁸, D. Krpic¹⁸, D. Maletic, J. Puzovic¹⁸, N. Smiljkovic

Centro de Investigaciones Energéticas Medioambientales y Tecnológicas (CIEMAT), Madrid, Spain

M. Aguilar-Benitez, J. Alberdi, J. Alcaraz Maestre, P. Arce, J.M. Barcala, C. Battilana, C. Burgos Lazaro, J. Caballero Bejar, E. Calvo, M. Cardenas Montes, M. Cepeda, M. Cerrada, M. Chamizo Llatas, F. Clemente, N. Colino, M. Daniel, B. De La Cruz, A. Delgado Peris, C. Diez Pardos, C. Fernandez Bedoya, J.P. Fernández Ramos, A. Ferrando, J. Flix, M.C. Fouz, P. Garcia-Abia, A.C. Garcia-Bonilla, O. Gonzalez Lopez, S. Goy Lopez, J.M. Hernandez, M.I. Josa, J. Marin, G. Merino, J. Molina, A. Molinero, J.J. Navarrete, J.C. Oller, J. Puerta Pelayo, L. Romero, J. Santaolalla, C. Villanueva Munoz, C. Willmott, C. Yuste

Universidad Autónoma de Madrid, Madrid, Spain

C. Albajar, M. Blanco Otano, J.F. de Trocóniz, A. Garcia Raboso, J.O. Lopez Berengueres

Universidad de Oviedo, Oviedo, Spain

J. Cuevas, J. Fernandez Menendez, I. Gonzalez Caballero, L. Lloret Iglesias, H. Naves Sordo, J.M. Vizan Garcia

Instituto de Física de Cantabria (IFCA), CSIC-Universidad de Cantabria, Santander, Spain

I.J. Cabrillo, A. Calderon, S.H. Chuang, I. Diaz Merino, C. Diez Gonzalez, J. Duarte Campderros, M. Fernandez, G. Gomez, J. Gonzalez Sanchez, R. Gonzalez Suarez, C. Jorda, P. Lobelle Pardo, A. Lopez Virto, J. Marco, R. Marco, C. Martinez Rivero, P. Martinez Ruiz del Arbol, F. Matorras, T. Rodrigo, A. Ruiz Jimeno, L. Scodellaro, M. Sobron Sanudo, I. Vila, R. Vilar Cortabitarte

CERN, European Organization for Nuclear Research, Geneva, Switzerland

D. Abbaneo, E. Albert, M. Alidra, S. Ashby, E. Auffray, J. Baechler, P. Baillon, A.H. Ball, S.L. Bally, D. Barney, F. Beaudette¹⁹, R. Bellan, D. Benedetti, G. Benelli, C. Bernet, P. Bloch, S. Bolognesi, M. Bona, J. Bos, N. Bourgeois, T. Bourrel, H. Breuker, K. Bunkowski, D. Campi, T. Camporesi, E. Cano, A. Cattai, J.P. Chatelain, M. Chauvey, T. Christiansen, J.A. Coarasa Perez, A. Conde Garcia, R. Covarelli, B. Curé, A. De Roeck, V. Delachenal, D. Deyrail, S. Di Vincenzo²⁰, S. Dos Santos, T. Dupont, L.M. Edera, A. Elliott-Peisert, M. Eppard, M. Favre, N. Frank, W. Funk, A. Gaddi, M. Gastal, M. Gateau, H. Gerwig, D. Gigi, K. Gill, D. Giordano, J.P. Girod, F. Glege, R. Gomez-Reino Garrido, R. Goudard, S. Gowdy, R. Guida, L. Guiducci, J. Gutleber, M. Hansen, C. Hartl, J. Harvey, B. Hegner, H.F. Hoffmann, A. Holzner, A. Honma, M. Huhtinen, V. Innocente, P. Janot, G. Le Godec, P. Lecoq, C. Leonidopoulos, R. Loos, C. Lourenço, A. Lyonnet, A. Macpherson, N. Magini, J.D. Maillefaud, G. Maire, T. Mäki, L. Malgeri, M. Mannelli, L. Masetti, F. Meijers, P. Meridiani, S. Mersi, E. Meschi, A. Meynet Cordonnier, R. Moser, M. Mulders, J. Mulon, M. Noy, A. Oh, G. Olesen, A. Onnela, T. Orimoto, L. Orsini, E. Perez, G. Perinic, J.F. Pernot, P. Petagna, P. Petiot, A. Petrilli, A. Pfeiffer, M. Pierini, M. Pimiä, R. Pintus, B. Pirollet, H. Postema, A. Racz, S. Ravat, S.B. Rew, J. Rodrigues Antunes, G. Rolandi²¹, M. Rovere, V. Ryjov, H. Sakulin, D. Samyn, H. Sauce, C. Schäfer, W.D. Schlatter, M. Schröder, C. Schwick, A. Sciaba, I. Segoni, A. Sharma, N. Siegrist, P. Siegrist, N. Sinanis, T. Sobrier, P. Sphicas²², D. Spiga, M. Spiropulu¹⁷, F. Stöckli, P. Traczyk, P. Tropea, J. Troska, A. Tsirou, L. Veillet, G.I. Veres, M. Voutilainen, P. Wertelaers, M. Zanetti

Paul Scherrer Institut, Villigen, Switzerland

W. Bertl, K. Deiters, W. Erdmann, K. Gabathuler, R. Horisberger, Q. Ingram, H.C. Kaestli, S. König, D. Kotlinski, U. Langenegger, F. Meier, D. Renker, T. Rohe, J. Sibille²³, A. Starodumov²⁴

Institute for Particle Physics, ETH Zurich, Zurich, Switzerland

B. Betev, L. Caminada²⁵, Z. Chen, S. Cittolin, D.R. Da Silva Di Calafiori, S. Dambach²⁵, G. Dissertori, M. Dittmar, C. Eggel²⁵, J. Eugster, G. Faber, K. Freudenreich, C. Grab, A. Hervé, W. Hintz, P. Lecomte, P.D. Luckey, W. Lustermann, C. Marchica²⁵, P. Milenovic²⁶, F. Moortgat, A. Nardulli, F. Nessi-Tedaldi, L. Pape, F. Pauss, T. Punz, A. Rizzi, F.J. Ronga, L. Sala, A.K. Sanchez, M.-C. Sawley, V. Sordini, B. Stieger, L. Tauscher[†], A. Thea, K. Theofilatos, D. Treille, P. Trüb²⁵, M. Weber, L. Wehrli, J. Weng, S. Zelepoukine²⁷

Universität Zürich, Zurich, Switzerland

C. Amsler, V. Chiochia, S. De Visscher, C. Regenfus, P. Robmann, T. Rommerskirchen, A. Schmidt, D. Tsirigkas, L. Wilke

National Central University, Chung-Li, Taiwan

Y.H. Chang, E.A. Chen, W.T. Chen, A. Go, C.M. Kuo, S.W. Li, W. Lin

National Taiwan University (NTU), Taipei, Taiwan

P. Bartalini, P. Chang, Y. Chao, K.F. Chen, W.-S. Hou, Y. Hsiung, Y.J. Lei, S.W. Lin, R.-S. Lu, J. Schümann, J.G. Shiu, Y.M. Tzeng, K. Ueno, Y. Velikzhanin, C.C. Wang, M. Wang

Cukurova University, Adana, Turkey

A. Adiguzel, A. Ayhan, A. Azman Gokce, M.N. Bakirci, S. Cerci, I. Dumanoglu, E. Eskut, S. Girgis, E. Gurpinar, I. Hos, T. Karaman, T. Karaman, A. Kayis Topaksu, P. Kurt, G. Öngüt, G. Öngüt Gökbulut, K. Ozdemir, S. Ozturk, A. Polatöz, K. Sogut²⁸, B. Tali, H. Topakli, D. Uzun, L.N. Vergili, M. Vergili

Middle East Technical University, Physics Department, Ankara, Turkey

I.V. Akin, T. Aliev, S. Bilmis, M. Deniz, H. Gamsizkan, A.M. Guler, K. Öcalan, M. Serin, R. Sever, U.E. Surat, M. Zeyrek

Bogaçi University, Department of Physics, Istanbul, Turkey

M. Deliomeroglu, D. Demir²⁹, E. Gülmez, A. Halu, B. Isildak, M. Kaya³⁰, O. Kaya³⁰, S. Ozkorucuklu³¹, N. Sonmez³²

National Scientific Center, Kharkov Institute of Physics and Technology, Kharkov, Ukraine

L. Levchuk, S. Lukyanenko, D. Soroka, S. Zub

University of Bristol, Bristol, United Kingdom

F. Bostock, J.J. Brooke, T.L. Cheng, D. Cussans, R. Frazier, J. Goldstein, N. Grant, M. Hansen, G.P. Heath, H.F. Heath, C. Hill, B. Huckvale, J. Jackson, C.K. Mackay, S. Metson, D.M. Newbold³³, K. Nirunpong, V.J. Smith, J. Velthuis, R. Walton

Rutherford Appleton Laboratory, Didcot, United Kingdom

K.W. Bell, C. Brew, R.M. Brown, B. Camanzi, D.J.A. Cockerill, J.A. Coughlan, N.I. Geddes, K. Harder, S. Harper, B.W. Kennedy, P. Murray, C.H. Shepherd-Themistocleous, I.R. Tomalin, J.H. Williams[†], W.J. Womersley, S.D. Worm

Imperial College, University of London, London, United Kingdom

R. Bainbridge, G. Ball, J. Ballin, R. Beuselinck, O. Buchmuller, D. Colling, N. Cripps, G. Davies, M. Della Negra, C. Foudas, J. Fulcher, D. Futyan, G. Hall, J. Hays, G. Iles, G. Karapostoli, B.C. MacEvoy, A.-M. Magnan, J. Marrouche, J. Nash, A. Nikitenko²⁴, A. Papageorgiou, M. Pesaresi, K. Petridis, M. Pioppi³⁴, D.M. Raymond, N. Rompotis, A. Rose, M.J. Ryan, C. Seez, P. Sharp, G. Sidiropoulos¹, M. Stettler, M. Stoye, M. Takahashi, A. Tapper, C. Timlin, S. Tourneur, M. Vazquez Acosta, T. Virdee¹, S. Wakefield, D. Wardrope, T. Whyntie, M. Wingham

Brunel University, Uxbridge, United Kingdom

J.E. Cole, I. Goitom, P.R. Hobson, A. Khan, P. Kyberd, D. Leslie, C. Munro, I.D. Reid, C. Siamitros, R. Taylor, L. Teodorescu, I. Yaselli

Boston University, Boston, U.S.A.

T. Bose, M. Carleton, E. Hazen, A.H. Heering, A. Heister, J. St. John, P. Lawson, D. Lazic, D. Osborne, J. Rohlf, L. Sulak, S. Wu

Brown University, Providence, U.S.A.

J. Andrea, A. Avetisyan, S. Bhattacharya, J.P. Chou, D. Cutts, S. Esen, G. Kukartsev, G. Landsberg, M. Narain, D. Nguyen, T. Speer, K.V. Tsang

University of California, Davis, Davis, U.S.A.

R. Breedon, M. Calderon De La Barca Sanchez, M. Case, D. Cebra, M. Chertok, J. Conway, P.T. Cox, J. Dolen, R. Erbacher, E. Friis, W. Ko, A. Kopecky, R. Lander, A. Lister, H. Liu, S. Maruyama, T. Miceli, M. Nikolic, D. Pellett, J. Robles, M. Searle, J. Smith, M. Squires, J. Stilley, M. Tripathi, R. Vasquez Sierra, C. Veelken

University of California, Los Angeles, Los Angeles, U.S.A.

V. Andreev, K. Arisaka, D. Cline, R. Cousins, S. Erhan¹, J. Hauser, M. Ignatenko, C. Jarvis, J. Mumford, C. Plager, G. Rakness, P. Schlein[†], J. Tucker, V. Valuev, R. Wallny, X. Yang

University of California, Riverside, Riverside, U.S.A.

J. Babb, M. Bose, A. Chandra, R. Clare, J.A. Ellison, J.W. Gary, G. Hanson, G.Y. Jeng, S.C. Kao, F. Liu, H. Liu, A. Luthra, H. Nguyen, G. Pasztor³⁵, A. Satpathy, B.C. Shen[†], R. Stringer, J. Sturdy, V. Sytnik, R. Wilken, S. Wimpenny

University of California, San Diego, La Jolla, U.S.A.

J.G. Branson, E. Dusinger, D. Evans, F. Golf, R. Kelley, M. Lebourgeois, J. Letts, E. Lipeles, B. Mangano, J. Muelmenstaedt, M. Norman, S. Padhi, A. Petrucci, H. Pi, M. Pieri, R. Ranieri, M. Sani, V. Sharma, S. Simon, F. Würthwein, A. Yagil

University of California, Santa Barbara, Santa Barbara, U.S.A.

C. Campagnari, M. D'Alfonso, T. Danielson, J. Garberson, J. Incandela, C. Justus, P. Kalavase, S.A. Koay, D. Kovalskyi, V. Krutelyov, J. Lamb, S. Lowette, V. Pavlunin, F. Rebassoo, J. Ribnik, J. Richman, R. Rossin, D. Stuart, W. To, J.R. Vlimant, M. Witherell

California Institute of Technology, Pasadena, U.S.A.

A. Apresyan, A. Bornheim, J. Bunn, M. Chiorboli, M. Gataullin, D. Kcira, V. Litvine, Y. Ma, H.B. Newman, C. Rogan, V. Timciuc, J. Veverka, R. Wilkinson, Y. Yang, L. Zhang, K. Zhu, R.Y. Zhu

Carnegie Mellon University, Pittsburgh, U.S.A.

B. Akgun, R. Carroll, T. Ferguson, D.W. Jang, S.Y. Jun, M. Paulini, J. Russ, N. Terentyev, H. Vogel, I. Vorobiev

University of Colorado at Boulder, Boulder, U.S.A.

J.P. Cumalat, M.E. Dinardo, B.R. Drell, W.T. Ford, B. Heyburn, E. Luiggi Lopez, U. Nauenberg, K. Stenson, K. Ulmer, S.R. Wagner, S.L. Zang

Cornell University, Ithaca, U.S.A.

L. Agostino, J. Alexander, F. Blekman, D. Cassel, A. Chatterjee, S. Das, L.K. Gibbons, B. Heltsley, W. Hopkins, A. Khukhunaishvili, B. Kreis, V. Kuznetsov, J.R. Patterson, D. Puigh, A. Ryd, X. Shi, S. Stoinev, W. Sun, W.D. Teo, J. Thom, J. Vaughan, Y. Weng, P. Wittich

Fairfield University, Fairfield, U.S.A.

C.P. Beetz, G. Cirino, C. Sanzeni, D. Winn

Fermi National Accelerator Laboratory, Batavia, U.S.A.

S. Abdullin, M.A. Afaq¹, M. Albrow, B. Ananthan, G. Apollinari, M. Atac, W. Badgett, L. Bagby, J.A. Bakken, B. Baldin, S. Banerjee, K. Banicz, L.A.T. Bauerdick, A. Beretvas, J. Berryhill, P.C. Bhat, K. Biery, M. Binkley, I. Bloch, F. Borcharding, A.M. Brett, K. Burkett, J.N. Butler, V. Chetluru, H.W.K. Cheung, F. Chlebana, I. Churin, S. Cihangir, M. Crawford, W. Dagenhart, M. Demarteau, G. Derylo, D. Dykstra, D.P. Eartly, J.E. Elias, V.D. Elvira, D. Evans, L. Feng, M. Fischler, I. Fisk, S. Foulkes, J. Freeman, P. Gartung, E. Gottschalk, T. Grassi, D. Green, Y. Guo, O. Gutsche, A. Hahn, J. Hanlon, R.M. Harris, B. Holzman, J. Howell, D. Hufnagel, E. James, H. Jensen, M. Johnson, C.D. Jones, U. Joshi, E. Juska, J. Kaiser, B. Klima, S. Kossakov, K. Kousouris, S. Kwan, C.M. Lei, P. Limon, J.A. Lopez Perez, S. Los, L. Lueking, G. Lukhanin, S. Lusin¹, J. Lykken, K. Maeshima, J.M. Marraffino, D. Mason, P. McBride, T. Miao, K. Mishra, S. Moccia, R. Mommsen, S. Mrenna, A.S. Muhammad, C. Newman-Holmes, C. Noeding, V. O'Dell, O. Prokofyev, R. Rivera, C.H. Rivetta, A. Ronzhin, P. Rossman, S. Ryu, V. Sekhri, E. Sexton-Kennedy, I. Sfiligoi, S. Sharma, T.M. Shaw, D. Shpakov, E. Skup, R.P. Smith[†], A. Soha, W.J. Spalding, L. Spiegel, I. Suzuki, P. Tan, W. Tanenbaum, S. Tkaczyk¹, R. Trentadue¹, L. Uplegger, E.W. Vaandering, R. Vidal, J. Whitmore, E. Wicklund, W. Wu, J. Yarba, F. Yumiceva, J.C. Yun

University of Florida, Gainesville, U.S.A.

D. Acosta, P. Avery, V. Barashko, D. Bourilkov, M. Chen, G.P. Di Giovanni, D. Dobur, A. Drozdetskiy, R.D. Field, Y. Fu, I.K. Furic, J. Gartner, D. Holmes, B. Kim, S. Klimenko, J. Konigsberg, A. Korytov, K. Kotov, A. Kropivnitskaya, T. Kypreos, A. Madorsky, K. Matchev, G. Mitselmakher, Y. Pakhotin, J. Piedra Gomez, C. Prescott, V. Rapsevicius, R. Remington, M. Schmitt, B. Scurlock, D. Wang, J. Yelton

Florida International University, Miami, U.S.A.

C. Ceron, V. Gaultney, L. Kramer, L.M. Lebolo, S. Linn, P. Markowitz, G. Martinez, J.L. Rodriguez

Florida State University, Tallahassee, U.S.A.

T. Adams, A. Askew, H. Baer, M. Bertoldi, J. Chen, W.G.D. Dharmaratna, S.V. Gleyzer, J. Haas, S. Hagopian, V. Hagopian, M. Jenkins, K.F. Johnson, E. Prettnner, H. Prosper, S. Sekmen

Florida Institute of Technology, Melbourne, U.S.A.

M.M. Baarmand, S. Guragain, M. Hohlmann, H. Kalakhety, H. Mermerkaya, R. Ralich, I. Vodopyanov

University of Illinois at Chicago (UIC), Chicago, U.S.A.

B. Abelev, M.R. Adams, I.M. Anghel, L. Apanasevich, V.E. Bazterra, R.R. Betts, J. Callner, M.A. Castro, R. Cavanaugh, C. Dragoiu, E.J. Garcia-Solis, C.E. Gerber, D.J. Hofman, S. Khalatian, C. Mironov, E. Shabalina, A. Smoron, N. Varelas

The University of Iowa, Iowa City, U.S.A.

U. Akgun, E.A. Albayrak, A.S. Ayan, B. Bilki, R. Briggs, K. Cankocak³⁶, K. Chung, W. Clarida, P. Debbins, F. Duru, F.D. Ingram, C.K. Lae, E. McCliment, J.-P. Merlo, A. Mestvirishvili, M.J. Miller, A. Moeller, J. Nachtman, C.R. Newsom, E. Norbeck, J. Olson, Y. Onel, F. Ozok, J. Parsons, I. Schmidt, S. Sen, J. Wetzel, T. Yetkin, K. Yi

Johns Hopkins University, Baltimore, U.S.A.

B.A. Barnett, B. Blumenfeld, A. Bonato, C.Y. Chien, D. Fehling, G. Giurgiu, A.V. Gritsan, Z.J. Guo, P. Maksimovic, S. Rappoccio, M. Swartz, N.V. Tran, Y. Zhang

The University of Kansas, Lawrence, U.S.A.

P. Baringer, A. Bean, O. Grachov, M. Murray, V. Radicci, S. Sanders, J.S. Wood, V. Zhukova

Kansas State University, Manhattan, U.S.A.

D. Bandurin, T. Bolton, K. Kaadze, A. Liu, Y. Maravin, D. Onoprienko, I. Svintradze, Z. Wan

Lawrence Livermore National Laboratory, Livermore, U.S.A.

J. Gronberg, J. Hollar, D. Lange, D. Wright

University of Maryland, College Park, U.S.A.

D. Baden, R. Bard, M. Boutemur, S.C. Eno, D. Ferencek, N.J. Hadley, R.G. Kellogg, M. Kim, S. Kunori, K. Rossato, P. Rumerio, F. Santanastasio, A. Skuja, J. Temple, M.B. Tonjes, S.C. Tonwar, T. Toole, E. Twedt

Massachusetts Institute of Technology, Cambridge, U.S.A.

B. Alver, G. Bauer, J. Bendavid, W. Busza, E. Butz, I.A. Cali, M. Chan, D. D'Enterria, P. Everaerts, G. Gomez Ceballos, K.A. Hahn, P. Harris, S. Jaditz, Y. Kim, M. Klute, Y.-J. Lee, W. Li, C. Loizides, T. Ma, M. Miller, S. Nahn, C. Paus, C. Roland, G. Roland, M. Rudolph, G. Stephans, K. Sumorok, K. Sung, S. Vaurynovich, E.A. Wenger, B. Wyslouch, S. Xie, Y. Yilmaz, A.S. Yoon

University of Minnesota, Minneapolis, U.S.A.

D. Bailleux, S.I. Cooper, P. Cushman, B. Dahmes, A. De Benedetti, A. Dolgoplov, P.R. Dudero, R. Egeland, G. Franzoni, J. Haupt, A. Inyakin³⁷, K. Klapoetke, Y. Kubota, J. Mans, N. Mirman, D. Petyt, V. Rekovic, R. Rusack, M. Schroeder, A. Singovsky, J. Zhang

University of Mississippi, University, U.S.A.

L.M. Cremaldi, R. Godang, R. Kroeger, L. Perera, R. Rahmat, D.A. Sanders, P. Sonnek, D. Summers

University of Nebraska-Lincoln, Lincoln, U.S.A.

K. Bloom, B. Bockelman, S. Bose, J. Butt, D.R. Claes, A. Dominguez, M. Eads, J. Keller, T. Kelly, I. Kravchenko, J. Lazo-Flores, C. Lundstedt, H. Malbouisson, S. Malik, G.R. Snow

State University of New York at Buffalo, Buffalo, U.S.A.

U. Baur, I. Iashvili, A. Kharchilava, A. Kumar, K. Smith, M. Strang

Northeastern University, Boston, U.S.A.

G. Alverson, E. Barberis, O. Boeriu, G. Eulisse, G. Govi, T. McCauley, Y. Musienko³⁸, S. Muzaffar, I. Osborne, T. Paul, S. Reucroft, J. Swain, L. Taylor, L. Tuura

Northwestern University, Evanston, U.S.A.

A. Anastassov, B. Gobbi, A. Kubik, R.A. Ofierzynski, A. Pozdnyakov, M. Schmitt, S. Stoynev, M. Velasco, S. Won

University of Notre Dame, Notre Dame, U.S.A.

L. Antonelli, D. Berry, M. Hildreth, C. Jessop, D.J. Karmgard, T. Kolberg, K. Lannon, S. Lynch, N. Marinelli, D.M. Morse, R. Ruchti, J. Slaunwhite, J. Warchol, M. Wayne

The Ohio State University, Columbus, U.S.A.

B. Bylsma, L.S. Durkin, J. Gilmore³⁹, J. Gu, P. Killewald, T.Y. Ling, G. Williams

Princeton University, Princeton, U.S.A.

N. Adam, E. Berry, P. Elmer, A. Garmash, D. Gerbaudo, V. Halyo, A. Hunt, J. Jones, E. Laird, D. Marlow, T. Medvedeva, M. Mooney, J. Olsen, P. Piroué, D. Stickland, C. Tully, J.S. Werner, T. Wildish, Z. Xie, A. Zuranski

University of Puerto Rico, Mayaguez, U.S.A.

J.G. Acosta, M. Bonnett Del Alamo, X.T. Huang, A. Lopez, H. Mendez, S. Oliveros, J.E. Ramirez Vargas, N. Santacruz, A. Zatzerklyany

Purdue University, West Lafayette, U.S.A.

E. Alagoz, E. Antillon, V.E. Barnes, G. Bolla, D. Bortoletto, A. Everett, A.F. Garfinkel, Z. Gecse, L. Gutay, N. Ippolito, M. Jones, O. Koybasi, A.T. Laasanen, N. Leonardo, C. Liu, V. Maroussov, P. Merkel, D.H. Miller, N. Neumeister, A. Sedov, I. Shipsey, H.D. Yoo, Y. Zheng

Purdue University Calumet, Hammond, U.S.A.

P. Jindal, N. Parashar

Rice University, Houston, U.S.A.

V. Cuplov, K.M. Ecklund, F.J.M. Geurts, J.H. Liu, D. Maronde, M. Matveev, B.P. Padley, R. Redjimi, J. Roberts, L. Sabbatini, A. Tumanov

University of Rochester, Rochester, U.S.A.

B. Betchart, A. Bodek, H. Budd, Y.S. Chung, P. de Barbaro, R. Demina, H. Flacher, Y. Gotra, A. Harel, S. Korjenevski, D.C. Miner, D. Orbaker, G. Petrillo, D. Vishnevskiy, M. Zielinski

The Rockefeller University, New York, U.S.A.

A. Bhatti, L. Demortier, K. Goulianos, K. Hatakeyama, G. Lungu, C. Mesropian, M. Yan

Rutgers, the State University of New Jersey, Piscataway, U.S.A.

O. Atramentov, E. Bartz, Y. Gershtein, E. Halkiadakis, D. Hits, A. Lath, K. Rose, S. Schnetzer, S. Somalwar, R. Stone, S. Thomas, T.L. Watts

University of Tennessee, Knoxville, U.S.A.

G. Cerizza, M. Hollingsworth, S. Spanier, Z.C. Yang, A. York

Texas A&M University, College Station, U.S.A.

J. Asaadi, A. Aurisano, R. Eusebi, A. Golyash, A. Gurrola, T. Kamon, C.N. Nguyen, J. Pivarski, A. Safonov, S. Sengupta, D. Toback, M. Weinberger

Texas Tech University, Lubbock, U.S.A.

N. Akchurin, L. Berntzon, K. Gumus, C. Jeong, H. Kim, S.W. Lee, S. Popescu, Y. Roh, A. Sill, I. Volobouev, E. Washington, R. Wigmans, E. Yazgan

Vanderbilt University, Nashville, U.S.A.

D. Engh, C. Florez, W. Johns, S. Pathak, P. Sheldon

University of Virginia, Charlottesville, U.S.A.

D. Andelin, M.W. Arenton, M. Balazs, S. Boutle, M. Buehler, S. Conetti, B. Cox, R. Hirosky, A. Ledovskoy, C. Neu, D. Phillips II, M. Ronquest, R. Yohay

Wayne State University, Detroit, U.S.A.

S. Gollapinni, K. Gunthoti, R. Harr, P.E. Karchin, M. Mattson, A. Sakharov

University of Wisconsin, Madison, U.S.A.

M. Anderson, M. Bachtis, J.N. Bellinger, D. Carlsmith, I. Crotty[†], S. Dasu, S. Dutta, J. Efron, F. Feyzi, K. Flood, L. Gray, K.S. Grogg, M. Grothe, R. Hall-Wilton¹, M. Jaworski, P. Klabbers, J. Klukas, A. Lanaro, C. Lazaridis, J. Leonard, R. Loveless, M. Magrans de Abril, A. Mohapatra, G. Ott, G. Polese, D. Reeder, A. Savin, W.H. Smith, A. Sourkov⁴⁰, J. Swanson, M. Weinberg, D. Wenman, M. Wensveen, A. White

†: Deceased

- 1: Also at CERN, European Organization for Nuclear Research, Geneva, Switzerland
- 2: Also at Universidade Federal do ABC, Santo Andre, Brazil
- 3: Also at Soltan Institute for Nuclear Studies, Warsaw, Poland
- 4: Also at Université de Haute-Alsace, Mulhouse, France
- 5: Also at Centre de Calcul de l'Institut National de Physique Nucleaire et de Physique des Particules (IN2P3), Villeurbanne, France
- 6: Also at Moscow State University, Moscow, Russia
- 7: Also at Institute of Nuclear Research ATOMKI, Debrecen, Hungary
- 8: Also at University of California, San Diego, La Jolla, U.S.A.
- 9: Also at Tata Institute of Fundamental Research - HECR, Mumbai, India
- 10: Also at University of Visva-Bharati, Santiniketan, India
- 11: Also at Facolta' Ingegneria Universita' di Roma "La Sapienza", Roma, Italy
- 12: Also at Università della Basilicata, Potenza, Italy
- 13: Also at Laboratori Nazionali di Legnaro dell' INFN, Legnaro, Italy
- 14: Also at Università di Trento, Trento, Italy
- 15: Also at ENEA - Casaccia Research Center, S. Maria di Galeria, Italy
- 16: Also at Warsaw University of Technology, Institute of Electronic Systems, Warsaw, Poland
- 17: Also at California Institute of Technology, Pasadena, U.S.A.
- 18: Also at Faculty of Physics of University of Belgrade, Belgrade, Serbia
- 19: Also at Laboratoire Leprince-Ringuet, Ecole Polytechnique, IN2P3-CNRS, Palaiseau, France
- 20: Also at Alstom Contracting, Geneve, Switzerland
- 21: Also at Scuola Normale e Sezione dell' INFN, Pisa, Italy
- 22: Also at University of Athens, Athens, Greece
- 23: Also at The University of Kansas, Lawrence, U.S.A.
- 24: Also at Institute for Theoretical and Experimental Physics, Moscow, Russia
- 25: Also at Paul Scherrer Institut, Villigen, Switzerland
- 26: Also at Vinca Institute of Nuclear Sciences, Belgrade, Serbia
- 27: Also at University of Wisconsin, Madison, U.S.A.
- 28: Also at Mersin University, Mersin, Turkey
- 29: Also at Izmir Institute of Technology, Izmir, Turkey
- 30: Also at Kafkas University, Kars, Turkey
- 31: Also at Suleyman Demirel University, Isparta, Turkey
- 32: Also at Ege University, Izmir, Turkey

- 33: Also at Rutherford Appleton Laboratory, Didcot, United Kingdom
- 34: Also at INFN Sezione di Perugia; Universita di Perugia, Perugia, Italy
- 35: Also at KFKI Research Institute for Particle and Nuclear Physics, Budapest, Hungary
- 36: Also at Istanbul Technical University, Istanbul, Turkey
- 37: Also at University of Minnesota, Minneapolis, U.S.A.
- 38: Also at Institute for Nuclear Research, Moscow, Russia
- 39: Also at Texas A&M University, College Station, U.S.A.
- 40: Also at State Research Center of Russian Federation, Institute for High Energy Physics, Protvino, Russia